Author Manuscript

Author Manuscript

Author Manuscript

Author Manuscript

HHS Public Access

Author manuscript

J Immunol. Author manuscript; available in PMC 2022 August 15.

Published in final edited form as:

J Immunol. 2021 August 15; 207(4): 1150–1164. doi:10.4049/jimmunol.2001233.

Pathway-specific Defects in T, B, and NK cells and Age-dependent Development of High IgE in Mice Heterozygous for a CADINS-associated Dominant Negative CARD11 Allele

Shelby M. Hutcherson, **Jacquelyn R. Bedsaul**, **Joel L. Pomerantz***

Department of Biological Chemistry, Institute for Cell Engineering, The Johns Hopkins University School of Medicine, Baltimore, MD 21205, USA

Abstract

CARD11 is a multidomain scaffold protein required for normal activation of NF-κB, JNK, and mTOR during antigen receptor signaling. Germline CARD11 mutations cause at least three types of primary immunodeficiency including CARD11 deficiency, B cell expansion with NF-κB and T cell anergy (BENTA), and CARD11-associated atopy with dominant interference of NF-κB signaling (CADINS). CADINS is uniquely caused by heterozygous loss-of-function CARD11 alleles that act as dominant negatives. CADINS patients present with frequent respiratory and skin infections, asthma, allergies, and atopic dermatitis. However, precisely how a heterozygous dominant negative CARD11 allele leads to the development of this CADINS-specific cluster of symptoms remains poorly understood. To address this, we generated mice expressing the CARD11 R30W allele originally identified in patients. We find that CARD11$^{R30W/+}$ mice exhibit impaired signaling downstream of CARD11 that leads to defects in T, B, and NK cell function and immunodeficiency. CARD11$^{R30W/+}$ mice develop elevated serum IgE levels with 50% penetrance that becomes more pronounced with age, but do not develop spontaneous atopic dermatitis. CARD11$^{R30W/+}$ mice display reduced Treg numbers, but not the Th2 expansion observed in other mice with diminished CARD11 activity. Interestingly, the presence of mixed CARD11 oligomers in CARD11$^{R30W/+}$ mice causes more severe signaling defects in T cells than in B cells, and specifically impacts IFNγ production by NK cells, but not NK cell cytotoxicity. Our findings help explain the high susceptibility of CADINS patients to infection and suggest that the development of high serum IgE is not sufficient to induce overt atopic symptoms.

Introduction

Antigen recognition by T cell receptor (TCR) and B cell receptor (BCR) complexes triggers multiple branching signaling pathways that are crucial for lymphocyte activation, proliferation, and survival during the adaptive immune response. Impaired signaling through these pathways can lead to immunodeficiency, increasing susceptibility to infections and making them difficult to clear.

*Corresponding author: Joel L. Pomerantz, PhD, Department of Biological Chemistry, Institute for Cell Engineering, The Johns Hopkins University School of Medicine, Miller Research Building, Room 607, 733 N Broadway, Baltimore, MD 21205, Voice: 443-287-3100, Fax: 443-287-3109, joel.pomerantz@jhmi.edu.

Author Manuscript Author Manuscript Author Manuscript Author Manuscript

CARD11 is a multidomain scaffold protein that serves as a critical hub during antigen receptor signaling, integrating the signals it receives from antigen receptors on the surface of T and B cells and translating them into activation of the NF-κB, JNK, and mTOR pathways (1–10). At rest, CARD11 is kept in a closed, inactive state via an inhibitory domain (ID) that functions through four redundant repressive elements (REs) (11–13). Antigen receptor engagement relieves this autoinhibition through a poorly understood process, allowing CARD11 to undergo a conformational change into an open, active scaffold (14–16). CARD11 then coordinates the recruitment and activation of a variety of cofactors including Bcl10, MALT1, HOIP, and many others (1, 11, 17–21). The assembly of this multiprotein complex and the activation of its components lead to the activation of IKK kinase activity, the phosphorylation and degradation of the inhibitory protein IκBα, and the subsequent nuclear translocation of NF-κB. The CARD11-nucleated complex also dictates the activation of JNK2 and mTORC1 (1).

The signal-inducible scaffold function of CARD11 is essential for normal antigen receptor signaling, and mutations that disrupt this function can impair the adaptive immune response. In the last several years, germline mutations in the CARD11 gene have been found to be responsible for at least three types of primary immunodeficiency (PID) in humans: CARD11 deficiency, B cell expansion with NF-κB and T cell anergy (BENTA), and CARD11-associated atopy with dominant interference of NF-κB signaling (CADINS) (1, 22–24). CARD11 deficiency is caused by homozygous loss-of-function (LOF) mutations in CARD11, and the 7 patients reported thus far presented with severe *Pneumocystis jirovecii* pneumonia, hypogammaglobulinemia and poor *in vitro* T and B cell activation despite having normal lymphocyte counts (24–29). BENTA is caused by heterozygous gain-of-function (GOF) mutations in CARD11 and is characterized by a massive expansion of B cells as well as recurrent viral infections and weak B and T cell responses to antigen challenges (30–36). CADINS is caused by heterozygous LOF mutations in CARD11 that act in a dominant negative manner to interfere with the function of the co-expressed wild type (WT) CARD11 allele (37–40). Patients with this condition exhibit an enhanced susceptibility to infections as well as a cohort of allergy-related symptoms known collectively as atopy.

In the last few years, at least 14 different dominant negative CARD11 mutations have been reported in 45 CADINS patients from nearly 20 unrelated families (37–40). The majority (12/14) of these variants are located throughout the CARD and Coiled-coil domains of CARD11, while the remaining 2 variants are located in the C-terminal guanylate kinase (GUK) domain. Nearly all of the patients presented with some form of atopy, with the most common symptoms being severe atopic dermatitis, asthma, and food and/or environmental allergies. In addition, laboratory tests revealed elevated serum IgE levels and high eosinophil counts in most patients. Despite having normal lymphocyte numbers, a history of viral skin infections such as molluscum contagiosum was also commonly reported, as well as recurrent respiratory tract infections, bouts of pneumonia, and bronchiectasis. Functional studies in patient lymphocytes have shown defective lymphocyte activation, poor responses to antigen challenges, and attenuated signaling to NF-κB and, to a lesser extent, mTORC1. However, these functional studies have only been performed in less than half of the

Author Manuscript Author Manuscript Author Manuscript Author Manuscript

patients. A fuller understanding of precisely how dominant negative CARD11 alleles lead to immunodeficiency and atopy is needed.

Here, we investigate the impact of a dominant negative CARD11 allele on the immune system using a mouse model expressing the CARD11 R30W mutation from the endogenous locus. The CARD11 R30W allele was first characterized in 4 patients from the same family who all presented with immunodeficiency and atopy (38). Subsequently, as part of a larger study, a 5th patient was identified (39). Studies on patient lymphocytes have shown impaired T cell activation and weak responses to various antigens and mitogens as compared to lymphocytes taken from healthy controls. However, it is difficult to determine whether the observed patient phenotypes are affected by confounding factors, such as environmental exposures, past and current treatments for symptoms, and the possible presence of modifier genes. In this report, we use CARD11$^{R30W/+}$ mice to examine how a dominant negative CARD11 mutation disrupts immune cell signaling and effector functions in the absence of these confounding factors. We show that heterozygous presence of the CARD11 R30W allele has diverse effects on both the signaling pathways downstream of CARD11 and the activation and function of T cells, B cells, and natural killer (NK) cells, leading to immunodeficiency and an incompletely penetrant age-dependent increase in serum IgE.

Materials and Methods

Mice

The CARD11 R30W allele was generated using CRISPR/Cas9 genome editing (41). A synthetic crRNA was designed to target the sequence 5'-TGTAACGGCTCAGCATGTGC-3'. The DNA oligonucleotide used as a template for homology-directed repair (HDR) was 5'-GACTACATG GAGACGCTGAAGGATGAAGAGGAGGCCCTATGGGATAACGTGGAATGCAAC**t**GGC ACATGCTGAGCCGTTACATCAACCCCGCCAAGCTCACCCCCTACCTGCGCCAGTG C-3' (lowercase letter indicates mutation). Introduction of the mutation removed an endogenous BsrFαI restriction site and introduced a novel BsrI restriction site. The crRNA, tracrRNA, recombinant Cas9, and HDR repair template oligo were injected into C57BL/6J embryos generated by the Transgenic Core Laboratory at the Johns Hopkins University School of Medicine. PCR followed by overnight digestion with BsrI or BsrFαI was performed on DNA from the resulting cohort of 41 live pups to determine which mice carried the CARD11 R30W mutation. The region surrounding R30 in the CARD domain of CARD11 was sequenced in these mice to confirm the presence of the CARD11 R30W allele, and two founders were selected based on the sequencing results. Founders were crossed to C57BL/6J mice, and germline transmission of the CARD11 R30W allele was confirmed in this and all subsequent generations via PCR followed by overnight BsrI or BsrFαI digestion. All mice used in experiments were at least 6 weeks of age. Mice were matched by age, sex, and litter within experiments whenever possible. All mice were maintained and all mouse procedures were conducted in accordance with the Johns Hopkins University Institutional Animal Care and Use Committee.

Author Manuscript Author Manuscript Author Manuscript Author Manuscript

Antibodies

Antibodies used for Western blotting and co-immunoprecipitations were as follows: mouse mAb against phospho-IκBα S32/S36 (5A5, 9246), rabbit polyclonal antibody against IκBα (9242), rabbit mAb against phospho-IKKα/β S176/S177 (C84E11, 2078S), rabbit polyclonal antibody against IKKβ (2684), rabbit mAb against GAPDH (D16H11, 5174), rabbit mAb against CARD11 (1D12, 4435), rabbit polyclonal antibody against phospho-SAPK/JNK T183/Y185 (9251), rabbit polyclonal antibody against JNK2 (4672), rabbit mAb against c-Jun (60A8, 9165), rabbit mAb against phospho-S6 S235/S236 (D57.2.2E, 4858), rabbit mAb against phospho-S6 S240/S244 (D68F8, 5364), and rabbit mAb against S6 (5G10, 2217) were from Cell Signaling Technology. Mouse mAb against HOIL-1 (H-1, sc-393754), mouse mAb against CYLD (E-10, sc-74435), and mouse mAb against Bcl10 (331.3, sc-5273) were from Santa Cruz Biotechnology.

Immunizations and antibody responses

Mice were immunized by intraperitoneal injection between 8 and 12 weeks of age with 25 μg DNP-Ficoll (Biosearch Technologies) in PBS or 50 μg DNP-CGG (Biosearch Technologies) precipitated in Imject Alum (Thermo Scientific). Blood samples were taken prior to immunization as well as 7 and 14 days after immunization. Serum was isolated from whole blood by allowing blood to clot at room temperature for 20 min, then centrifuging at 2000×g for 10 min at 4°C. Antibody responses were measured by DNP-specific ELISA. Diluted serum was incubated on plates coated with 5 μg/mL DNP-BSA (Biosearch Technologies), and DNP-specific antibodies were detected using HRP-conjugated secondary antibodies against the indicated mouse isotypes.

Western blotting

Spleens were harvested into RPMI 1640 media supplemented with 10% FBS and 2% penicillin/streptomycin/L-glutamine and dissociated using the frosted side of glass microscope slides. Single-cell suspensions were obtained by passing dissociated organs over a 70 μm cell strainer. Red blood cells were lysed with ACK lysis buffer (Quality Biological) and the final cell pellet was resuspended in 1x PBS for counting. $CD4^+$ T cells, B cells, or NK cells were purified from whole splenocytes by negative selection using the mouse $CD4^+$ T cell Isolation Kit, Pan B Cell Isolation Kit II, or NK Cell Isolation Kit (Miltenyi Biotec) according to the manufacturer's instructions. T cells and B cells were stimulated directly after isolation, while NK cells were expanded in supplemented RPMI containing 50 ng/mL recombinant mouse IL-15 (PeproTech 210-15) for 6 days prior to stimulation. A total of 2×10^6 T, B, or NK cells were resuspended in supplemented RPMI and allowed to rest for 30 min at 37°C, then stimulated for the indicated times at 37°C with 1 μg/mL hamster anti-mouse CD3 (145-2C11, BD 553058), 2 μg/mL hamster anti-mouse CD28 (37.51, BD 553295), and 1 μg/mL mouse anti-hamster IgG1 (HIG-632, BD 550637), 25 nM PMA (Sigma) and 62.5 nM ionomycin (Sigma), or 0.1 μg/mL anti-mouse IgM (Invitrogen 16-5092-85). Cells were incubated for 10 min on ice, spun at 5000 rpm for 5 min, and lysed in 30 μL immunoprecipitation lysis buffer (IPLB) (11) containing protease inhibitor cocktail (Sigma P8340) alone or with Halt phosphatase inhibitor cocktail (Thermo Scientific). Samples were heat-treated at 95°C in SDS loading buffer, resolved via

Author Manuscript Author Manuscript Author Manuscript Author Manuscript

SDS-PAGE, and transferred to polyvinylidene difluoride membranes. Western blotting was performed with the indicated antibodies and protein bands were quantified using ImageJ software. The results shown are representative of at least two replicates of each experiment.

Endogenous co-immunoprecipitation

Spleens were harvested and processed as described above. T cells or B cells were purified from whole splenocytes by negative selection using the mouse $CD4^+$ T cell Isolation Kit or Pan B Cell Isolation Kit II (Miltenyi Biotec) according to the manufacturer's instructions. Purified T or B cells were resuspended in supplemented RPMI and allowed to rest for 30 min at 37°C, then stimulated with 100 nM PMA (Sigma) and 1 μM ionomycin (Sigma) for 30 min at 37°C. Cells were incubated for 10 min on ice, spun at 1400 rpm for 5 min, and lysed in 1 mL IPLB with protease inhibitor cocktail (Sigma P8340). Lysates were incubated with 2 μg mouse anti-Bcl10 antibody for 4 h at 4°C with rotation, then incubated with 20 μL bed volume of native protein A-conjugated Sepharose (GE Healthcare) overnight at 4°C with rotation. Immunoprecipitates were washed four times for 10 min at 4°C with rotation. Immunoprecipitates and cell lysate input samples were heat-treated at 95°C in SDS loading buffer, resolved by SDS-PAGE, and transferred to polyvinylidene difluoride membranes. Western blotting was performed with the indicated antibodies.

Flow cytometry

Organs were harvested and processed as described above. For measuring lymphocyte numbers and thymic T cell development, whole splenocytes or thymocytes were washed in FACS buffer (PBS, pH 7.4, 0.5% BSA, 2 mM EDTA, 0.02% sodium azide), then stained in FACS buffer for 30 min on ice with CD19-APC-Cy7 (1D3, BD), B220-PerCP-Cy5.5 (RA3-6B2, BD), CD3-APC (145-2C11, BD), CD4-BV421 (GK1.5, BD), CD8-FITC (53–6.7, BD), TER-119-APC-Cy7 (TER-119, BD), Gr-1-APC-Cy7 (RB6-8C5, BD), NK1.1-PE (PK136, BD), and CD49b-Pacific Blue (DX5, Biolegend). For measuring upregulation of activation markers, T cells or B cells were purified from whole splenocytes by negative selection using the mouse $CD4^+$ T Cell Isolation Kit or Pan B Cell Isolation Kit II (Miltenyi Biotec) according to the manufacturer's instructions. A total of 1×10^5 cells per sample were stimulated in 96-well plates in supplemented RPMI with or without the indicated concentrations of plate-bound hamster anti-mouse CD3 (145-2C11, BD 553058) and 2 μg/mL hamster anti-mouse CD28 (37.51, BD 553295) for T cells or anti-mouse IgM (Invitrogen 16-5092-85) for B cells. Cells were washed in FACS buffer and surface stained in FACS buffer for 30 min on ice with CD25-APC (PC61, BD) for T cells or CD86-BV421 (GL-1, Biolegend) for B cells. For peritoneal B1 cell staining, peritoneal cavity cells were isolated by peritoneal lavage with 5 mL 1x PBS + 3% FBS. Cells were washed with FACS buffer, then incubated in Fc block (2.4G2, BD) for 10 min at room temperature. After washing again in FACS buffer, cells were stained in FACS buffer for 30 min on ice with CD11b-BV421 (M1/70, BD), B220-PerCP-Cy5.5 (RA3-6B2, BD), CD5-APC (53-7.3, BD), and IgM-PE (RMM-1, Biolegend). For staining of marginal zone and follicular B cells, whole splenocytes were washed with FACS buffer, then incubated in Fc block (2.4G2, BD) for 10 min at room temperature. After washing again in FACS buffer, cells were stained in FACS buffer with CD19-APC-Cy7 (1D3, BD), B220-PerCP-Cy5.5 (RA3-6B2, BD), IgM-PE-Cy7 (R6-60.2, BD), IgD-APC (11-26c.2a, BD), CD21-FITC (7E9, Biolegend), and

Author Manuscript Author Manuscript Author Manuscript Author Manuscript

CD23-PE (B3B4, BD). For Treg staining, 1×10^6 whole splenocytes or thymocytes per sample were plated in 96-well round-bottom plates and stained with Live/Dead Aqua fixable viability dye (Invitrogen) in 1x PBS for 30 min at room temperature, then washed with FACS buffer. Cells were surface stained in FACS buffer for 10 min at room temperature with CD3-FITC (145-2C11, BD), CD4-BV-421 (GK1.5, BD), CD8-PE-Cy7 (53-6.7, BD), and CD25-APC (PC61, BD), then fixed and permeabilized using the FoxP3/Transcription Factor Staining Buffer Set (Invitrogen). Intracellular staining for FoxP3-PE (FJK-16s, Invitrogen) was performed in 1x permeabilization buffer for 30 min on ice. Cells were washed twice in 1x permeabilization buffer, then resuspended in FACS buffer for data collection. All flow cytometry data was collected on a BD LSR II or BD FACSCelesta flow cytometer and analyzed using FlowJo software (TreeStar).

ELISAs

For cytokine ELISAs, spleens were harvested and processed as described above. $CD4^+$ T cells, $CD8^+$ T cells, or NK cells were isolated from whole splenocytes using the mouse $CD4^+$ T Cell Isolation Kit, mouse $CD8a^+$ T Cell Isolation Kit, or NK Cell Isolation Kit (Miltenyi Biotec) according to the manufacturer's instructions. T cells were stimulated directly after isolation, while NK cells were either stimulated directly after isolation or expanded in supplemented RPMI containing 50 ng/mL recombinant mouse IL-15 (PeproTech 210-15) for 6 days prior to stimulation. A total of 1×10^5 (T cells) or 5×10^4 (NK cells) purified cells per sample were stimulated in 96-well plates in supplemented RPMI with or without the indicated concentrations of plate-bound hamster anti-mouse CD3 (145-2C11, BD 553058) and 2 μg/mL hamster anti-mouse CD28 (37.51, BD 553295) for T cells or 5 μg/mL anti-mouse NKG2D (A10, Invitrogen 16-5872-82) and 50 ng/mL recombinant human IL-2 (Biolegend 589104) for NK cells. After 24 h, culture supernatants were harvested by centrifugation at 1400 rpm for 5 min. Cytokine concentrations in culture supernatants were measured using the mouse IL-2 uncoated ELISA kit (Invitrogen 88-7024-88), mouse IFNγ uncoated ELISA kit (Invitrogen 88-7314-88), mouse IL-4 uncoated ELISA kit (Invitrogen 88-7044-88), or mouse IL-13 uncoated ELISA kit (Invitrogen 88-7137-88) according to the manufacturer's instructions. For serum ELISAs, serum was isolated from whole blood as described above. The amount of the indicated immunoglobulin isotypes in serum samples was measured using the mouse IgE uncoated ELISA kit (Invitrogen 88-50460-88), mouse IgM uncoated ELISA kit (Invitrogen 88-50470-88), mouse IgG1 uncoated ELISA kit (Invitrogen 88-50410-88), mouse IgG2a uncoated ELISA kit (Invitrogen 88-50420-88), mouse IgG2b uncoated ELISA kit (Invitrogen 88-50430-88), or mouse IgG3 uncoated ELISA kit (Invitrogen 88-50440-88).

$CD4^+$ T cell skewing in vitro

Spleens were harvested and processed as described above. Naïve $CD4^+$ T cells were purified from whole splenocytes by negative selection using the mouse Naïve $CD4^+$ T Cell Isolation Kit (Miltenyi Biotec) according to the manufacturer's instructions. A total of 2×10^6 cells per sample were stimulated in 24-well plates in supplemented RPMI with 1 μg/mL plate-bound hamster anti-mouse CD3 (145-2C11, BD 553058) and 1 μg/mL plate-bound hamster anti-mouse CD28 (37.51, BD 553295) for 2 days. For Th1 skewing, cultures contained 10 ng/mL mouse IL-12, 10 ng/mL mouse IL-2, and 10 μg/mL anti-IL-4 (Cytobox Th1,

Author Manuscript Author Manuscript Author Manuscript Author Manuscript

Miltenyi Biotec). For Th2 skewing, cultures contained 10 ng/mL mouse IL-4, 10 ng/mL mouse IL-2, and 10 μg/mL anti-IFNγ (Cytobox Th2, Miltenyi Biotec). On day 2, cells were removed from the stimuli and split 1:4 in media containing fresh skewing cytokines and antibodies. On day 4, cells were washed with PBS, counted, and 1×10^5 cells per sample were restimulated with 1 μg/mL plate-bound hamster anti-mouse CD3. After 24 h, culture supernatants were harvested by centrifugation at 1400 rpm for 5 min and the concentrations of IFNγ, IL-4, and IL-13 were measured by ELISA using the kits described above.

MC903 model of atopic dermatitis

Induction of atopic dermatitis-like skin inflammation via topical application of MC903 was performed as previously described (42). MC903 (Tocris 2700) was used at a working concentration of 45 μM. Mice were anesthetized via isoflurane inhalation and 12.5 μL MC903 or 100% ethanol was pipetted onto each side of an unpunched ear once daily in the following treatment sequence: 5 days treatment, 2 days no treatment, 5 days treatment, 2 days no treatment, 2 days treatment. Mice were sacrificed 24 hours after the last treatment and 6 mm punch biopsies of the treated ear tissue were harvested along with the draining lymph node. The 6 mm punch biopsies were bisected, and one half was fixed in 10% formalin and embedded in paraffin. Skin cross sections were prepared and stained with hematoxylin and eosin by the Johns Hopkins Reference Histology Laboratory. Images were taken at 20x magnification on an Olympus BX51 microscope with an Olympus DP70 color camera and ImageJ software was used to measure epidermal thickness. The other half of the punch biopsy was homogenized in TPER Tissue Protein Extraction Reagent (Thermo Scientific) containing protease inhibitor cockatil (Sigma P8340). The protein concentration in the homogenate was determined using a Pierce BCA Protein Assay Kit (Thermo Fisher 23227), and 40 μg protein per sample was used to measure the concentration of IFNγ and IL-4 in the homogenates by ELISA using the kits described above. The draining lymph node was processed as described above for the spleen. Cells were washed with FACS buffer, then stained in FACS buffer for 30 min on ice with CD11b-BV421 (M1/70, BD), CD4-PerCP-Cy5.5 (RM 4–5, Invitrogen), Siglec F-PE (E50-2440, BD), Ly6C-FITC (AL-21, BD), and Ly6G-APC (1A8, BD). Flow cytometry was performed on a BD FACSCelesta flow cytometer and data was analyzed using FlowJo software (Treestar).

YAC-1 lysis assay

Spleens were harvested and processed as described above. NK cells were purified from whole splenocytes by negative selection using the mouse NK Cell Isolation Kit (Miltenyi Biotec) according to the manufacturer's instructions. Purity of isolated NK cells was assessed via flow cytometry by staining for NK1.1-PE (PK136, BD) and CD49b (DX5, Biolegend). The YAC-1 lysis assay was performed as described previously (43). YAC-1 cells were loaded with 500 nM CellTrace CFSE (Invitrogen) according to the manufacturer's instructions. Equivalent numbers of $NK1.1^+CD49b^+$ NK cells were co-cultured in 96-well plates with CFSE-loaded YAC-1 cells in the indicated E:T ratios for 4 h. Cells were then stained with Annexin V and analyzed via flow cytometry. YAC-1 lysis was calculated as the percentage of $CFSE^+$Annexin V^+ cells and is reported as the percentage of specific lysis.

Author Manuscript Author Manuscript Author Manuscript Author Manuscript

Results

A single copy of the CARD11 R30W allele is sufficient to cause immunodeficiency

To investigate the impact of a dominant negative CARD11 allele on the immune system, we generated mice bearing the CARD11 R30W allele using CRISPR/Cas9 genome editing in single-cell zygotes (41). CARD11$^{R30W/+}$ mice were born in Mendelian ratios, appeared healthy, and had normal numbers of splenocytes and thymocytes (Figure S1a–b). Our initial examination of cell populations in CARD11$^{R30W/+}$ mice also showed normal numbers of splenic B cells, CD4^{+} T cells, CD8^{+} T cells, and NK cells (Figure S1c–f). CARD11$^{R30W/+}$ mice exhibited no significant differences from WT in thymic double-negative, double-positive, and single-positive T cells, suggesting normal T cell development (Figure S1g). Patients heterozygous for the dominant negative CARD11 R30W mutation show enhanced susceptibility to a variety of infections and reduced ability to clear their infections (38, 39). To determine whether the CARD11 R30W mutation is sufficient to cause immunodeficiency in the absence of other modifier genes or environmental effects, we immunized WT and CARD11$^{R30W/+}$ mice with model antigens and monitored the levels of antigen-specific serum antibodies over the course of two weeks. When immunized with the T-independent antigen DNP-Ficoll, WT mice exhibited a robust response, producing large quantities of DNP-specific IgM and IgG3 at both day 7 and day 14 post-injection. In contrast, CARD11$^{R30W/+}$ mice failed to produce detectable levels of both antigen-specific isotypes throughout the course of the experiment (Figure 1a). We also immunized mice with DNP-CGG, a protein antigen that requires T cell help for the production of antigen-specific antibodies. DNP-specific IgM, IgG1, and IgG2a were found in the serum of immunized WT mice 7 days after immunization, and the levels of all three isotypes had increased further on day 14. CARD11$^{R30W/+}$ mice were able to produce some DNP-specific antibodies against this antigen, but their response varied by isotype and was generally weaker or delayed relative to WT mice (Figure 1b). For example, the DNP-IgM response in CARD11$^{R30W/+}$ mice was delayed compared to the response in WT mice, with lower levels of DNP-IgM detected on day 7 post-injection but levels similar to WT detected on day 14. The same delayed response was observed in CARD11$^{R30W/+}$ mice when measuring DNP-IgG1, while the DNP-IgG2a response was clearly reduced at both time points. These results indicate that a heterozygous dominant negative CARD11 R30W mutation is sufficient to cause immunodeficiency in the absence of other mutations or environmental factors.

The CARD11 R30W allele severely impairs T cell activation and signaling

To investigate the basis for immunodeficiency in mice bearing the CARD11 R30W mutation, we assessed T cell activation in response to stimulation with αCD3/αCD28. We isolated splenic CD4^{+} T cells from WT, CARD11$^{R30W/+}$, and CARD11$^{R30W/R30W}$ mice, stimulated with increasing amounts of αCD3 while holding the concentration of αCD28 constant, and measured IL-2 production by ELISA. We found that while WT T cells showed strong secretion of IL-2 even at low concentrations of αCD3, CARD11$^{R30W/+}$ T cells failed to produce any detectable IL-2 even at the highest concentration of αCD3 tested (Figure 2a). We observed the same profound defect when measuring IFNγ production by CARD11$^{R30W/+}$ CD8^{+} T cells stimulated in the same manner (Figure 2b). We also measured the upregulation of the high-affinity IL-2 receptor subunit CD25 upon stimulation in purified

Author Manuscript Author Manuscript Author Manuscript Author Manuscript

$CD4^+$ T cells via flow cytometry. CD25 was readily upregulated on the surface of WT T cells, and its signal increased steadily with the concentration of αCD3 used for stimulation. $CARD11^{R30W/+}$ T cells were able to upregulate CD25 slightly at higher concentrations of αCD3, but the signal was consistently about 2-fold lower than in WT T cells. Furthermore, $CARD11^{R30W/R30W}$ T cells showed a complete defect in CD25 upregulation (Figure 2c–d). These data indicate that even one copy of the CARD11 R30W mutation confers severe defects in T cell activation.

We next examined the effect of the CARD11 R30W mutation on the CARD11-associated signaling pathways underlying T cell activation. We isolated and stimulated splenic $CD4^+$ T cells, then probed key steps of multiple signaling pathways via Western blotting. Signaling to NF-κB was severely impaired in $CARD11^{R30W/+}$ T cells relative to WT T cells, as indicated by a 4.7-fold decrease in peak signal-induced IKKα/β phosphorylation, a 5.5-fold decrease in peak IκBα phosphorylation, and reduced IκBα degradation (Figure 2e–f). We also observed a 2.2-fold and 2.5-fold reduction in peak MALT1-mediated cleavage of its substrates HOIL-1 and CYLD, respectively (Figure 2g–h), and completely defective signal-inducible binding of Bcl10 to CARD11 (Figure 2i–j). T cells from heterozygous mice express both wild type and mutant CARD11 proteins that assemble into mixed oligomers of undetermined stoichiometry. These results indicate that the presence of the CARD11 R30W mutant in mixed oligomers impairs the ability of CARD11 to interact with and activate its cofactors during induced signaling in primary T cells.

Signaling through JNK2 was also disrupted in $CARD11^{R30W/+}$ T cells, as indicated by a 5.9-fold decrease in peak phosphorylation of JNK2 compared to WT T cells (Figure 2k–l). However, accumulation of the transcription factor c-Jun was largely unaffected by the CARD11 R30W mutation, likely because JNK1 can still be phosphorylated and lead to c-Jun accumulation independently of CARD11 (44). In patient studies, dominant negative CARD11 alleles have been associated with defective mTOR signaling in some cases, but not others. Unlike the NF-κB and JNK pathways, we found only a modest 1.6-fold reduction in peak phosphorylation of the ribosomal protein S6 in $CARD11^{R30W/+}$ T cells when measuring signaling through mTORC1 (Figure 2m–n). The profound signaling defects observed in $CARD11^{R30W/+}$ mice provide an explanation for the observed deficits in T cell activation and in turn, for aspects of their immunodeficiency.

The CARD11 R30W allele has only a mild impact on B cell activation and signaling

To assess the effect of the heterozygous CARD11 R30W mutation on B cell function, we isolated splenic B cells from WT, $CARD11^{R30W/+}$, and $CARD11^{R30W/R30W}$ mice, stimulated them with increasing concentrations of αIgM, and measured upregulation of the activation marker CD86 by flow cytometry after 24 hours. We detected no difference in surface IgM expression between WT and $CARD11^{R30W/+}$ B cells (Figure S2). The level of CD86 detected on the surface of WT B cells increased steadily with the concentration of αIgM used for stimulation. While $CARD11^{R30W/+}$ B cells exhibited slightly reduced upregulation of CD86 at higher concentrations of αIgM, this phenotype was not as severe as the defect in CD25 upregulation observed in $CARD11^{R30W/+}$ T cells upon stimulation. In addition, $CARD11^{R30W/R30W}$ B cells exhibited a slight reduction in CD86 upregulation

Author Manuscript Author Manuscript Author Manuscript Author Manuscript

that was similar to the heterozygous B cells (Figure 3a–b). The effect of the heterozygous CARD11 R30W mutation on CARD11-associated signaling pathways was also weaker in B cells than in $CD4^+$ T cells. In the NF-κB pathway, peak phosphorylation of IκBα and phosphorylation of IKKα/β were reduced by 1.4-fold and 2.0-fold respectively in $CARD11^{R30W/+}$ B cells relative to WT B cells (Figure 3c–d) with no significant effect on IκBα degradation. Peak MALT1-mediated proteolysis of HOIL-1 and CYLD was not significantly reduced in $CARD11^{R30W/+}$ B cells (Figure 3e–f), but inducible Bcl10 binding to CARD11 was completely abrogated (Figure 3g–h). Peak phosphorylation of JNK2 was only decreased by 1.2-fold in $CARD11^{R30W/+}$ B cells after 15 minutes of stimulation but was reduced by 6.3-fold after 30 minutes of stimulation and 16-fold after 60 minutes of stimulation. c-Jun accumulation remained largely stable, as in T cells (Figure 3i–j). Signaling through mTORC1 was not reduced in $CARD11^{R30W/+}$ B cells, as indicated by levels of S6 phosphorylation comparable to WT (Figure 3k–l). These data indicate that the branching pathways downstream of CARD11 are differentially affected by the presence of CARD11 R30W in mixed CARD11 oligomers in B and T lymphocytes.

Reduced serum IgM and age-dependent elevation of serum IgE with incomplete penetrance in $CARD11^{R30W/+}$ mice

Given their diminished production of antigen-specific antibodies, we next sought to determine whether $CARD11^{R30W/+}$ mice would display altered basal immunoglobulin profiles. Of the 4 patients heterozygous for the CARD11 R30W allele who had their immunoglobulins measured, 2 were found to have low serum IgM or IgG, and this phenotype is also common in patients bearing other dominant negative CARD11 alleles (37–39). We measured basal levels of IgM, IgG2b, and IgG3 in the serum of WT and $CARD11^{R30W/+}$ mice by ELISA and found that the levels of IgG2b and IgG3 in $CARD11^{R30W/+}$ serum samples were normal, but the level of IgM was reduced 4.8-fold relative to WT mice (Figure 4a). To investigate the basis for the observed decrease in basal serum IgM levels, we used flow cytometry to examine the B1a and B1b B cell populations in the peritoneal cavity of WT and $CARD11^{R30W/+}$ mice, since these “innate-like” B cells are thought to be a major source of secreted IgM in mice (45, 46). We discovered that $CARD11^{R30W/+}$ mice had 3.9-fold fewer peritoneal $CD5^+IgM^+$ B1a cells on average than their WT counterparts, while $CD5^-IgM^+$ B1b cell numbers were similar in both genotypes (Figure 4b–c). Because marginal zone B cells are another important source of secreted IgM (47, 48), we also assessed marginal zone and follicular B cell populations in the spleens of WT and $CARD11^{R30W/+}$ mice and found that $CARD11^{R30W/+}$ mice had 2.0-fold fewer splenic marginal zone B cells than WT mice (Figure 4d–e). Follicular B cell numbers, however, were not significantly different in WT and $CARD11^{R30W/+}$ mice (Figure 4f–g). These results provide an explanation for the reduced IgM in $CARD11^{R30W/+}$ mice and indicate that a dominant negative CARD11 allele can impact both peritoneal B1a cell and splenic marginal zone B cell numbers.

In addition to their immunodeficiency, patients heterozygous for the CARD11 R30W mutation also exhibit elevated serum IgE and atopy, manifested as atopic dermatitis, asthma, and food and environmental allergies (38, 39). To determine whether the CARD11 R30W mutation is sufficient to cause these phenotypes in the absence of modifier genes

Author Manuscript Author Manuscript Author Manuscript Author Manuscript

and environmental exposures, we measured basal IgE levels in the serum of WT and CARD11$^{R30W/+}$ mice by ELISA. In CARD11$^{R30W/+}$ mice less than 10 weeks old, serum IgE was 2.0-fold higher than WT levels on average, but this 2.0-fold increase was primarily due to the presence of 2 mice of 16 assayed that showed 10- to 15-fold increases over WT IgE values (Figure 4h). This prompted us to examine IgE levels in older mice as well. We found that among CARD11$^{R30W/+}$ mice between 10 and 20 weeks of age, a larger percentage had elevated serum IgE, leading to a 2.2-fold average increase over WT values (Figure 4i). Furthermore, we detected massively elevated serum IgE in 50% of CARD11$^{R30W/+}$ mice older than 20 weeks of age, with the average IgE measurement approximately 13-fold higher than in WT mice (Figure 4j). The increases in serum IgE occurred in equal proportions in male and female mice, indicating a lack of sex-dependence. These results show that one copy of the CARD11 R30W mutation is sufficient to cause elevated serum IgE that becomes progressively more pronounced with age, but with only 50% penetrance. Interestingly, although 50% of CARD11$^{R30W/+}$ mice developed elevated serum IgE levels as they aged, none of these mice developed atopic dermatitis.

Loss of Tregs in CARD11$^{R30W/+}$ mice does not lead to expansion of Th2 cells

Previous studies have examined the effect of a homozygous hypomorphic CARD11 mutation, L298Q, in the *unmodulated* mouse strain (7, 49). *Unmodulated* mice also exhibit elevated serum IgE, but they develop spontaneous atopic dermatitis as they age. These phenotypes in *unmodulated* mice have been attributed to a substantially reduced regulatory T cell population that leads to the progressive expansion of Th2 cells, which secrete cytokines that promote B cell class switching and in turn lead to elevated IgE levels and atopic dermatitis (49). To assess whether there is a similar basis for the development of elevated IgE in CARD11$^{R30W/+}$ mice, we assessed the Treg population in the spleen and thymus of WT, CARD11$^{R30W/+}$, and CARD11$^{R30W/R30W}$ mice. We found that in the spleen and the thymus, CARD11$^{R30W/+}$ mice had 4.4-fold and 3.9-fold fewer Tregs than WT mice, respectively (Figure 5a–d). CARD11$^{R30W/R30W}$ mice almost completely lacked Tregs, with a 63-fold reduction in Treg numbers in the spleen and a 96-fold reduction in the thymus relative to WT mice (Figure 5a–d).

To determine whether the reduction in Treg numbers in CARD11$^{R30W/+}$ mice might lead to the expansion of Th2 cells, we isolated CD4^{+} T cells from WT and CARD11$^{R30W/+}$ mice less than 10 weeks old, stimulated them, and measured cytokine production by ELISA, using IFNγ as a signature Th1 cytokine and IL-4 and IL-13 as signature Th2 cytokines. CARD11$^{R30W/+}$ T cells exhibited substantial defects in production of IFNγ, IL-4, and IL-13 relative to WT T cells, indicating that the isolated splenic T cells had not obviously skewed to a Th2 state in CARD11$^{R30W/+}$ mice (Figure 5e). Similarly, when we skewed naïve CD4^{+} T cells to Th1 and Th2 subtypes in culture, we observed defective production of IFNγ, IL-4, and IL-13 in CARD11$^{R30W/+}$ Th1 and Th2 cells compared to WT cells (Figure 5f). Finally, we assessed whether Th2 cells were more prevalent in CARD11$^{R30W/+}$ mice that had already developed elevated IgE. We isolated CD4^{+} T cells from WT mice, CARD11$^{R30W/+}$ mice that had aged with normal IgE, and CARD11$^{R30W/+}$ mice that had aged with high IgE, stimulated them, and measured Th1 and Th2 cytokine production by ELISA. Once again, we found that IFNγ, IL-4, and IL-13 production was suboptimal in isolated CD4^{+} T cells

Author Manuscript Author Manuscript Author Manuscript Author Manuscript

from CARD11$^{R30W/+}$ mice as compared to those from WT mice, regardless of whether the mouse had concomitant high serum IgE (Figure 5g). Together, these results indicate that CARD11$^{R30W/+}$ mice exhibit deficits in both Th1 and Th2 cytokine production and do not show a propensity to skew toward a Th2 state such as what has been observed in the *unmodulated* mouse.

CARD11$^{R30W/+}$ mice do not exhibit enhanced susceptibility to atopic dermatitis-like inflammation driven by topical application of the vitamin D analog MC903

The lack of spontaneous atopic dermatitis in CARD11$^{R30W/+}$ mice prompted us to test whether these mice might exhibit an enhanced inflammatory response in a model of induced atopic dermatitis. If so, the behavior could reveal the possibility that a dominant negative CARD11 allele could predispose mice toward an atopic response in the skin. Therefore, we assayed the response of CARD11$^{R30W/+}$ mice to topical application of the vitamin D analog MC903, which triggers the overexpression of the cytokine thymic stromal lymphopoietin (TSLP) in keratinocytes (42, 50). TSLP acts as an alarmin, initiating a Th2-dominant immune response that leads to the development of atopic dermatitis-like symptoms (51). We applied MC903 or 100% ethanol vehicle to the ears of WT and CARD11$^{R30W/+}$ mice over the course of 16 days, then harvested tissue from the treated ears to assess inflammation. Visible signs of inflammation such as redness, scaling, and increased vascularization began to appear in mouse ears treated with MC903 after about 5–7 days of treatment and grew progressively worse as the treatment course continued, while mouse ears treated with ethanol alone appeared grossly normal throughout the treatment course. Tissue biopsies of ears treated with MC903 weighed substantially more than biopsies of ear tissue treated with ethanol, indicating swelling, but tissue from WT and CARD11$^{R30W/+}$ mice treated with MC903 had similar weights (Figure 6a). H&E staining of the ear tissue showed that MC903 treatment caused massive infiltration of immune cells into the dermis and thickening of the epidermis, but epidermal thickening occurred to a similar degree in both WT and CARD11$^{R30W/+}$ mice (Figure 6b–c). Likewise, ELISAs on ear tissue lysates for Th1 and Th2 cytokines showed that MC903 treatment caused a dramatic increase in both IFNγ and IL-4 levels compared to ethanol treatment, and CARD11$^{R30W/+}$ cytokine levels were comparable to WT levels (Figure 6d). We also harvested the draining lymph node from mice treated with MC903 and ethanol and found that lymph nodes from MC903-treated mice were also swollen, containing an average of 14-fold more total cells than lymph nodes from ethanol-treated mice. CARD11$^{R30W/+}$ lymph nodes treated with MC903 were slightly smaller than their WT counterparts, but this difference was not statistically significant (Figure 6e). We used flow cytometry to measure the infiltration of CD4^{+} T cells, eosinophils, monocytes, and neutrophils into the draining lymph node and found that while MC903 treatment led to a large influx of immune cells into the lymph node, there were no significant differences in the numbers of any immune cell subset in the lymph nodes of treated WT or CARD11$^{R30W/+}$ mice (Figure 6f). Taken together, these results indicate that the CARD11 R30W allele does not lead to an enhanced inflammatory response to TSLP release in the skin in the MC903 model of induced atopic dermatitis.

Author Manuscript Author Manuscript Author Manuscript Author Manuscript

The CARD11 R30W allele impairs inflammatory cytokine production by NK cells without affecting cytotoxicity

Given the stark signaling and functional deficits observed in CARD$^{R30W/+}$ B cells and T cells, we next sought to determine whether the CARD11 R30W mutation impacts NK cell function. CARD11 is expressed in NK cells and has been shown to coordinate NF-κB activation downstream of their activating receptors (52, 53), but the possibility that a dominant negative CARD11 allele could influence NK cell function has not been addressed. To assess the effect of the heterozygous CARD11 R30W mutation on inflammatory cytokine secretion, we isolated splenic NK cells from WT, CARD11$^{R30W/+}$, and CARD11$^{R30W/R30W}$ mice, stimulated with αNKG2D and IL-2 for 24 hours, and measured the production of IFNγ by ELISA. We found that the amount of secreted IFNγ decreased as the number of copies of the CARD11 R30W mutation increased. CARD11$^{R30W/+}$ NK cells exhibited a 1.7-fold reduction in IFNγ production relative to WT NK cells, while CARD11$^{R30W/R30W}$ NK cells exhibited a 5.0-fold reduction (Figure 7a). We observed similar decreases in IFNγ secretion by NK cells harboring the CARD11 R30W mutation when using NK cells that were expanded in culture in the presence of IL-15 for 6 days prior to stimulation (Figure 7b). To assess how the CARD11 R30W mutation affects NK cell cytotoxicity, we employed an NK cell killing assay using the YAC-1 lymphoma cell line as target (43, 54). We co-cultured CFSE-loaded YAC-1 cells with equal numbers of freshly isolated splenic NK cells (NK1.1$^+$CD49b$^+$) from WT, CARD11$^{R30W/+}$, or CARD11$^{R30W/R30W}$ mice in a range of effector:target (E:T) ratios for four hours, then used Annexin V to stain for dead cells and measured the number of CFSE$^+$Annexin V$^+$ cells via flow cytometry. NK cells from CARD11$^{R30W/+}$ and CARD11$^{R30W/R30W}$ mice lysed the target YAC-1 cells just as efficiently as WT NK cells across the full spectrum of E:T ratios (Figure 7c), indicating that the CARD11 R30W mutation specifically impairs cytokine secretion downstream of NKG2D without affecting cytotoxicity.

The defect we observed in cytokine production by CARD11$^{R30W/+}$ NK cells prompted us to assess the effect of the CARD11 R30W allele on signaling to NF-κB in these cells. We isolated splenic NK cells from WT and CARD11$^{R30W/+}$ mice, expanded them in culture in the presence of IL-15 for 6 days, stimulated them with PMA and ionomycin to mimic signaling downstream of NK receptors, including NKG2D, that couple to ITAM-containing NK adapters (52), and evaluated activation of the NF-κB pathway by Western blotting. Peak phosphorylation of IKKα/β was reduced by 11-fold in CARD11$^{R30W/+}$ NK cells, while peak IκBα phosphorylation was decreased by 14-fold and IκBα degradation was markedly impaired (Figure 7d–e). Together, these results indicate that the CARD11 R30W allele severely impairs signaling to NF-κB in NK cells, leading to reduced inflammatory cytokine production without affecting cytotoxicity.

Discussion

At least three forms of primary immunodeficiency are caused by germline mutations in the CARD11 gene including CARD11 deficiency, caused by homozygous LOF mutations, BENTA, caused by heterozygous GOF mutations, and CADINS, caused by heterozygous LOF dominant negative mutations. While all three syndromes involve an

Author Manuscript Author Manuscript Author Manuscript Author Manuscript

enhanced susceptibility to infection, CADINS uniquely involves a high incidence of atopy accompanied by a range of clinical presentations that can differ from patient to patient (37–40, 55). In an effort to study the impact of a dominant negative LOF CARD11 allele in the absence of the modifier genes, environmental exposures, and treatment regimens that could influence the presentation of CADINS patients, we generated and characterized mice heterozygous for the CARD11 R30W mutation identified in one of the initial CADINS families (38). Our results reveal that a single dominant negative CARD11 allele is sufficient to cause pathway-specific defects in the T, B and NK cell lineages, leading to defective immune responses and an age-dependent dramatic increase in serum IgE without the spontaneous atopic dermatitis and Th2 expansion observed in other mice with diminished CARD11 function.

CARD11 signals as an oligomer of undetermined stoichiometry. Previous studies have characterized the effects of diminished CARD11 function in CARD11-deficient mice, which express no CARD11 oligomer at all (5, 6, 52, 53, 56), or in homozygous *unmodulated* mice, which express CARD11 oligomers composed solely of hypomorphic mutant subunits that retain some signaling potential (7, 49). Both CARD11-deficient and *unmodulated* mice have defects in antigen-induced T cell and B cell activation and in TCR and BCR signaling to NF-κB and JNK. Both strains also display reduced Treg numbers, but in contrast to CARD11-deficient mice, *unmodulated* mice retain enough CARD11 signaling in lymphocytes to allow a scenario in which reduced Treg function promotes a skewing of T cells to a Th2 phenotype that induces class switching in B cells, leading to hyper IgE production and atopic dermatitis (49). The $CARD11^{R30W/+}$ mice we have generated have provided the opportunity to examine the phenotypic consequences of mixed CARD11 oligomers composed of wild-type subunits and mutant subunits that are loss-of-function and act in a dominant negative manner to reduce signaling from the wild-type subunits in the same oligomer.

Our data show that such mixed oligomers have different effects depending on the cellular context and the pathway downstream of CARD11, leading to an overall phenotype that appears different from CARD11-deficient and *unmodulated* mice and that expands our understanding of CARD11 signaling. We observed a greater apparent effect of mixed CARD11 oligomers on antigen receptor signaling to NF-κB in $CD4^+$ T cells than in B cells in the first 30 minutes of signaling, despite the fact that in both cell types the co-expression of wild-type and mutant CARD11 is sufficient to prevent the inducible formation of the CBM complex as reflected in Bcl10 recruitment to CARD11. The data suggest that in this early phase of signaling, antigen-mediated activation of NF-κB is much less dependent on CBM complex formation in B cells than it is in $CD4^+$ T cells, raising the likelihood that BCR signaling activates NF-κB through previously unrecognized mechanisms. We also observed greater effects of mixed WT:R30W CARD11 oligomers on signaling to JNK in T cells than in B cells, and mTOR signaling was only mildly reduced by the mixed oligomers in T cells and not reduced at all in B cells. The data highlight the need for further mechanistic study to fully understand the differences in antigen receptor signaling steps in T and B cells and uncover what aspects of the T and B cell environments make signaling pathways downstream of CARD11 more susceptible to mixed CARD11 oligomers in T cells than in B cells.

Author Manuscript Author Manuscript Author Manuscript Author Manuscript

While early CARD11 signaling to NF-κB, JNK and mTOR is largely intact in CARD11$^{R30W/+}$ B cells, the mixed CARD11 oligomers clearly impact longer-term consequences of antigen receptor signaling in B cells. CARD11$^{R30W/+}$ mice exhibit a severely defective immune response to T-independent antigen and a delayed response to T-dependent antigen that generates lower amounts of antigen-specific serum IgG2a. The severely defective T-independent response likely reflects a more pronounced effect of mixed CARD11 oligomers in B1a and marginal zone B cells, which mediate this response (46, 57). Consistent with this, we observed significant selective reductions in these B cells populations in CARD11$^{R30W/+}$ mice.

Previous studies in CARD11-deficient mice have demonstrated a required role for CARD11 in NK cell cytokine secretion downstream of activating receptor engagement (52, 53). However, it was unclear whether a dominant negative CARD11 mutant assembled into mixed WT:mutant oligomers would impact NK cell function, especially since no studies of NK cells from CADINS patients have been reported. Our data reveal for the first time that mixed CARD11 oligomers disrupt NK cell function. CARD11$^{R30W/+}$ NK cells display a substantially reduced capacity to produce IFNγ upon stimulation with anti-NKG2D but show no reduced capacity to lyse YAC-1 target cells *in vitro*, even though YAC-1 killing by murine NK cells is partially dependent on NKG2D triggering (54). This specificity is consistent with previous studies in CARD11-deficient mice that demonstrated a specific requirement for CARD11 in NKG2D-mediated cytokine signaling, but not in cytotoxicity, attributable to a role for CARD11 downstream of the DAP12 ITAM-containing adapter (52). We also observed that mixed WT:R30W CARD11 oligomers severely perturb signaling to NF-κB induced by PMA/ionomycin treatment, which mimics PKC-dependent signaling downstream of ITAM-coupled receptors on NK cells. Since human NK cells are also activated by NKG2D triggering and by other receptors that signal through ITAM-containing adapters, the data suggest that NK cell defects could contribute to the high susceptibility of patients with dominant negative CARD11 alleles to viral infections and that NK function should be examined in such patients.

The development of atopy in patients with dominant negative CARD11 mutations is not well understood. While their diminished lymphocyte function is sufficient to cause immunodeficiency, the residual immune function present appears to be abnormally skewed, yielding atopic symptoms in nearly 90% of patients (39). It remains mysterious to what extent the atopy results from cell-intrinsic defects in lymphocyte development and behavior, whether the high IgE observed in patients is sufficient to induce atopy, whether modifier genes contribute, and whether environmental exposure to antigen or other factors play a role. Our data indicate that heterozygous presence of the CARD11 R30W mutation is sufficient to cause elevated serum IgE in an age-dependent manner with 50% penetrance. However, unlike in *unmodulated* mice (7, 49), the elevated IgE is not accompanied by atopic dermatitis. In addition, despite having reduced Treg numbers, CARD11$^{R30W/+}$ mice do not display an obvious skewing of CD4^{+} T cells to a Th2 state, either before or after the development of elevated IgE levels. Clearly high IgE is not sufficient to induce atopic symptoms. It is likely that exposure to antigens or pathogens in the environment are required for the induction of atopy in mice or patients heterozygous for a dominant negative CARD11 variant, and that a Th2 response triggered by factors other than reduced Treg activity plays

Author Manuscript Author Manuscript Author Manuscript Author Manuscript

a role. Consistent with this notion, most CADINS patients do not exhibit reductions in Treg numbers or suppressive capability (37, 39). The response of CARD11$^{R30W/+}$ mice to application of the vitamin D analog MC903 suggests that an enhanced response to TSLP release in the skin is not likely to be the basis for the atopic dermatitis observed in CADINS patients. It remains unclear why the development of high serum IgE in CARD11$^{R30W/+}$ mice is age-dependent and 50% penetrant. We did not observe any correlations between the development of high serum IgE and sex or cage co-occupancy, suggesting that the microbiome may not contribute to high IgE induction. The age-dependence and incomplete penetrance that we observed in CARD11$^{R30W/+}$ mice emphasizes that even in a controlled genetic and environmental setting, there is individual-to-individual variability in how a dominant negative CARD11 allele can predispose to an abnormal immunological response.

An increasing number of germline mutations have been recognized as the basis for primary immunodeficiency syndromes that are associated with IgE-related allergic disease (58). The CARD11$^{R30W/+}$ mice will be a useful tool to unravel the complex mechanisms by which incomplete immune system dampening elicits these syndromes.

Supplementary Material

Refer to Web version on PubMed Central for supplementary material.

Acknowledgments

We thank Chip Hawkins for performing zygote injections, Nathan Archer and Mollie Meffert for advice, and Nicole M. Carter and Tyler A. Jones for critical reading of the manuscript.

This work was supported by National Institutes of Health Grant RO1AI148143 and funds from The Johns Hopkins University Institute for Cell Engineering. SMH was supported by National Institutes of Health Grants T32GM007445 and T32CA009110. JRB was supported by National Institutes of Health Grant T32AI007247.

References

1. Bedsaul JR, Carter NM, Deibel KE, Hutcherson SM, Jones TA, Wang Z, Yang C, Yang YK, and Pomerantz JL. 2018. Mechanisms of Regulated and Dysregulated CARD11 Signaling in Adaptive Immunity and Disease. Front Immunol9: 2105. [PubMed: 30283447]
2. Gaide O, Favier B, Legler DF, Bonnet D, Brissoni B, Valitutti S, Bron C, Tschopp J, and Thome M. 2002. CARMA1 is a critical lipid raft-associated regulator of TCR-induced NF-kappa B activation. Nat. Immunol3: 836–843. [PubMed: 12154360]
3. Wang D, You Y, Case SM, McAllister-Lucas LM, Wang L, DiStefano PS, Nunez G, Bertin J, and Lin X. 2002. A requirement for CARMA1 in TCR-induced NF-kappa B activation. Nat. Immunol3: 830–835. [PubMed: 12154356]
4. Pomerantz JL, Denny EM, and Baltimore D. 2002. CARD11 mediates factor-specific activation of NF-kappaB by the T cell receptor complex. EMBO J21: 5184–5194. [PubMed: 12356734]
5. Hara H, Wada T, Bakal C, Kozieradzki I, Suzuki S, Suzuki N, Nghiem M, Griffiths EK, Krawczyk C, Bauer B, D'Acquisto F, Ghosh S, Yeh WC, Baier G, Rottapel R, and Penninger JM. 2003. The MAGUK family protein CARD11 is essential for lymphocyte activation. Immunity18: 763–775. [PubMed: 12818158]
6. Egawa T, Albrecht B, Favier B, Sunshine MJ, Mirchandani K, O'Brien W, Thome M, and Littman DR. 2003. Requirement for CARMA1 in antigen receptor-induced NF-kappa B activation and lymphocyte proliferation. Curr. Biol13: 1252–1258. [PubMed: 12867038]
7. Jun JE, Wilson LE, Vinuesa CG, Lesage S, Blery M, Miosge LA, Cook MC, Kucharska EM, Hara H, Penninger JM, Domashenz H, Hong NA, Glynne RJ, Nelms KA, and Goodnow CC. 2003.

Author Manuscript Author Manuscript Author Manuscript Author Manuscript

Identifying the MAGUK protein Carma-1 as a central regulator of humoral immune responses and atopy by genome-wide mouse mutagenesis. Immunity18: 751–762. [PubMed: 12818157]

8. Blonska M, Pappu BP, Matsumoto R, Li H, Su B, Wang D, and Lin X. 2007. The CARMA1-Bcl10 signaling complex selectively regulates JNK2 kinase in the T cell receptor-signaling pathway. Immunity26: 55–66. [PubMed: 17189706]
9. Hamilton KS, Phong B, Corey C, Cheng J, Gorentla B, Zhong X, Shiva S, and Kane LP. 2014. T cell receptor-dependent activation of mTOR signaling in T cells is mediated by Carma1 and MALT1, but not Bcl10. Sci Signal7: ra55. [PubMed: 24917592]
10. Nakaya M, Xiao Y, Zhou X, Chang JH, Chang M, Cheng X, Blonska M, Lin X, and Sun SC. 2014. Inflammatory T cell responses rely on amino acid transporter ASCT2 facilitation of glutamine uptake and mTORC1 kinase activation. Immunity40: 692–705. [PubMed: 24792914]
11. McCully RR, and Pomerantz JL. 2008. The protein kinase C-responsive inhibitory domain of CARD11 functions in NF-kappaB activation to regulate the association of multiple signaling cofactors that differentially depend on Bcl10 and MALT1 for association. Mol. Cell. Biol28: 5668–5686. [PubMed: 18625728]
12. Jattani RP, Tritapoe JM, and Pomerantz JL. 2016. Cooperative Control of Caspase Recruitment Domain-containing Protein 11 (CARD11) Signaling by an Unusual Array of Redundant Repressive Elements. J. Biol. Chem291: 8324–8336. [PubMed: 26884335]
13. Jattani RP, Tritapoe JM, and Pomerantz JL. 2016. Intramolecular Interactions and Regulation of Cofactor Binding by the Four Repressive Elements in the Caspase Recruitment Domain-containing Protein 11 (CARD11) Inhibitory Domain. J. Biol. Chem291: 8338–8348. [PubMed: 26884334]
14. Sommer K, Guo B, Pomerantz JL, Bandaranayake AD, Moreno-Garcia ME, Ovechkina YL, and Rawlings DJ. 2005. Phosphorylation of the CARMA1 linker controls NF-kappaB activation. Immunity23: 561–574. [PubMed: 16356855]
15. Matsumoto R, Wang D, Blonska M, Li H, Kobayashi M, Pappu B, Chen Y, Wang D, and Lin X. 2005. Phosphorylation of CARMA1 plays a critical role in T Cell receptor-mediated NF-kappaB activation. Immunity23: 575–585. [PubMed: 16356856]
16. Shinohara H, Maeda S, Watarai H, and Kurosaki T. 2007. IkappaB kinase beta-induced phosphorylation of CARMA1 contributes to CARMA1 Bcl10 MALT1 complex formation in B cells. J. Exp. Med204: 3285–3293. [PubMed: 18086859]
17. Yang YK, Yang C, Chan W, Wang Z, Deibel KE, and Pomerantz JL. 2016. Molecular Determinants of Scaffold-induced Linear Ubiquitinylation of B Cell Lymphoma/Leukemia 10 (Bcl10) during T Cell Receptor and Oncogenic Caspase Recruitment Domain-containing Protein 11 (CARD11) Signaling. J. Biol. Chem291: 25921–25936. [PubMed: 27777308]
18. Bidere N, Ngo VN, Lee J, Collins C, Zheng L, Wan F, Davis RE, Lenz G, Anderson DE, Arnoult D, Vazquez A, Sakai K, Zhang J, Meng Z, Veenstra TD, Staudt LM, and Lenardo MJ. 2009. Casein kinase 1alpha governs antigen-receptor-induced NF-kappaB activation and human lymphoma cell survival. Nature458: 92–96. [PubMed: 19118383]
19. Medeiros RB, Burbach BJ, Mueller KL, Srivastava R, Moon JJ, Highfill S, Peterson EJ, and Shimizu Y. 2007. Regulation of NF-kappaB activation in T cells via association of the adapter proteins ADAP and CARMA1. Science316: 754–758. [PubMed: 17478723]
20. Schimmack G, Eitelhuber AC, Vincendeau M, Demski K, Shinohara H, Kurosaki T, and Krappmann D. 2014. AIP augments CARMA1-BCL10-MALT1 complex formation to facilitate NF-kappaB signaling upon T cell activation. Cell Commun Signal12: 49. [PubMed: 25245034]
21. Wang Z, Hutcherson SM, Yang C, Jattani RP, Tritapoe JM, Yang YK, and Pomerantz JL. 2019. Coordinated regulation of scaffold opening and enzymatic activity during CARD11 signaling. J. Biol. Chem294: 14648–14660. [PubMed: 31391255]
22. Lu HY, Biggs CM, Blanchard-Rohner G, Fung SY, Sharma M, and Turvey SE. 2019. Germline CBM-opathies: From immunodeficiency to atopy. J. Allergy Clin. Immunol143: 1661–1673. [PubMed: 31060714]
23. Lu HY, Bauman BM, Arjunaraja S, Dorjbal B, Milner JD, Snow AL, and Turvey SE. 2018. The CBM-opathies-A Rapidly Expanding Spectrum of Human Inborn Errors of Immunity Caused by Mutations in the CARD11-BCL10-MALT1 Complex. Front Immunol9: 2078. [PubMed: 30283440]

Author Manuscript Author Manuscript Author Manuscript Author Manuscript

24. Turvey SE, Durandy A, Fischer A, Fung SY, Geha RS, Gewies A, Giese T, Greil J, Keller B, McKinnon ML, Neven B, Rozmus J, Ruland J, Snow AL, Stepensky P, and Warnatz K. 2014. The CARD11-BCL10-MALT1 (CBM) signalosome complex: Stepping into the limelight of human primary immunodeficiency. J. Allergy Clin. Immunol134: 276–284. [PubMed: 25087226]

25. Greil J, Rausch T, Giese T, Bandapalli OR, Daniel V, Bekeredjian-Ding I, Stutz AM, Drees C, Roth S, Ruland J, Korbel JO, and Kulozik AE. 2013. Whole-exome sequencing links caspase recruitment domain 11 (CARD11) inactivation to severe combined immunodeficiency. J. Allergy Clin. Immunol131: 1376–1383 e1373. [PubMed: 23561803]

26. Stepensky P, Keller B, Buchta M, Kienzler AK, Elpeleg O, Somech R, Cohen S, Shachar I, Miosge LA, Schlesier M, Fuchs I, Enders A, Eibel H, Grimbacher B, and Warnatz K. 2013. Deficiency of caspase recruitment domain family, member 11 (CARD11), causes profound combined immunodeficiency in human subjects. J. Allergy Clin. Immunol131: 477–485 e471. [PubMed: 23374270]

27. Fuchs S, Rensing-Ehl A, Pannicke U, Lorenz MR, Fisch P, Jeelall Y, Rohr J, Speckmann C, Vraetz T, Farmand S, Schmitt-Graeff A, Kruger M, Strahm B, Henneke P, Enders A, Horikawa K, Goodnow C, Schwarz K, and Ehl S. 2015. Omenn syndrome associated with a functional reversion due to a somatic second-site mutation in CARD11 deficiency. Blood126: 1658–1669. [PubMed: 26289640]

28. Lu HY, Sharma M, Sharma AA, Lacson A, Szpurko A, Luider J, Dharmani-Khan P, Shameli A, Bell PA, Guilcher GMT, Lewis VA, Vasquez MR, Desai S, McGonigle L, Murguia-Favela L, Wright NAM, Sergi C, Wine E, Overall CM, Suresh S, and Turvey SE. 2021. Mechanistic understanding of the combined immunodeficiency in complete human CARD11 deficiency. J. Allergy Clin. Immunol doi: 10.1016/j.jaci.2021.04.006.

29. Al-Rasheed B, Alazami AM, and Al-Mousa H. 2020. Phenoidentical HLA-Related Hematopoietic Stem Cell Transplant Without Conditioning to Reconstitute a Patient with a Putative Loss-of-Function CARD11 Mutation. J. Clin. Immunol40: 1163–1165. [PubMed: 32815076]

30. Snow AL, Xiao W, Stinson JR, Lu W, Chaigne-Delalande B, Zheng L, Pittaluga S, Matthews HF, Schmitz R, Jhavar S, Kuchen S, Kardava L, Wang W, Lamborn IT, Jing H, Raffeld M, Moir S, Fleisher TA, Staudt LM, Su HC, and Lenardo MJ. 2012. Congenital B cell lymphocytosis explained by novel germline CARD11 mutations. J. Exp. Med209: 2247–2261. [PubMed: 23129749]

31. Brohl AS, Stinson JR, Su HC, Badgett T, Jennings CD, Sukumar G, Sindiri S, Wang W, Kardava L, Moir S, Dalgard CL, Moscow JA, Khan J, and Snow AL. 2015. Germline CARD11 Mutation in a Patient with Severe Congenital B Cell Lymphocytosis. J. Clin. Immunol35: 32–46. [PubMed: 25352053]

32. Buchbinder D, Stinson JR, Nugent DJ, Heurtier L, Suarez F, Sukumar G, Dalgard CL, Masson C, Parisot M, Zhang Y, Matthews HF, Su HC, Durandy A, Fischer A, Kracker S, and Snow AL. 2015. Mild B-cell lymphocytosis in patients with a CARD11 C49Y mutation. J. Allergy Clin. Immunol136: 819–821 e811. [PubMed: 25930198]

33. Arjunaraja S, Angelus P, Su HC, and Snow AL. 2018. Impaired Control of Epstein-Barr Virus Infection in B-Cell Expansion with NF-kappaB and T-Cell Anergy Disease. Front Immunol9: 198. [PubMed: 29472930]

34. Arjunaraja S, Nose BD, Sukumar G, Lott NM, Dalgard CL, and Snow AL. 2017. Intrinsic Plasma Cell Differentiation Defects in B Cell Expansion with NF-kappaB and T Cell Anergy Patient B Cells. Front Immunol8: 913. [PubMed: 28824638]

35. Outinen T, Syrjanen J, Rounioja S, Saarela J, Kaustio M, and Helminen M. 2016. Constant B cell lymphocytosis since early age in a patient with CARD11 mutation: A 20-year follow-up. Clin. Immunol165: 19–20. [PubMed: 26861442]

36. Gupta M, Aluri J, Desai M, Lokeshwar M, Taur P, Lenardo M, Bergerson J, Dalvi A, Mhatre S, Kulkarni M, Kambli P, and Madkaikar M. 2018. Clinical, Immunological, and Molecular Findings in Four Cases of B Cell Expansion With NF-kappaB and T Cell Anergy Disease for the First Time From India. Front Immunol9: 1049. [PubMed: 29963038]

37. Ma CA, Stinson JR, Zhang Y, Abbott JK, Weinreich MA, Hauk PJ, Reynolds PR, Lyons JJ, Nelson CG, Ruffo E, Dorjbal B, Glauzy S, Yamakawa N, Arjunaraja S, Voss K, Stoddard J, Niemela J, Zhang Y, Rosenzweig SD, McElwee JJ, DiMaggio T, Matthews HF, Jones N, Stone KD, Palma A,

Author Manuscript Author Manuscript Author Manuscript Author Manuscript

Oleastro M, Prieto E, Bernasconi AR, Dubra G, Danielian S, Zaiat J, Marti MA, Kim B, Cooper MA, Romberg N, Meffre E, Gelfand EW, Snow AL, and Milner JD. 2017. Germline hypomorphic CARD11 mutations in severe atopic disease. Nat. Genet49: 1192–1201. [PubMed: 28628108]

38. Dadi H, Jones TA, Merico D, Sharfe N, Ovadia A, Schejter Y, Reid B, Sun M, Vong L, Atkinson A, Lavi S, Pomerantz JL, and Roifman CM. 2018. Combined immunodeficiency and atopy caused by a dominant negative mutation in caspase activation and recruitment domain family member 11 (CARD11). J. Allergy Clin. Immunol141: 1818–1830 e1812. [PubMed: 28826773]
39. Dorjbal B, Stinson JR, Ma CA, Weinreich MA, Miraghazadeh B, Hartberger JM, Frey-Jakobs S, Weidinger S, Moebus L, Franke A, Schaffer AA, Bulashevska A, Fuchs S, Ehl S, Limaye S, Arkwright PD, Briggs TA, Langley C, Bethune C, Whyte AF, Alachkar H, Nejentsev S, DiMaggio T, Nelson CG, Stone KD, Nason M, Brittain EH, Oler AJ, Veltri DP, Leahy TR, Conlon N, Poli MC, Borzutzky A, Cohen JI, Davis J, Lambert MP, Romberg N, Sullivan KE, Paris K, Freeman AF, Lucas L, Chandrakasan S, Savic S, Hambleton S, Patel SY, Jordan MB, Theos A, Lebensburger J, Atkinson TP, Torgerson TR, Chinn IK, Milner JD, Grimbacher B, Cook MC, and Snow AL. 2019. Hypomorphic caspase activation and recruitment domain 11 (CARD11) mutations associated with diverse immunologic phenotypes with or without atopic disease. J. Allergy Clin. Immunol143: 1482–1495. [PubMed: 30170123]
40. Izadi N, Bauman BM, Dabbah G, Thauland TJ, Butte MJ, Snow AL, and Church JA. 2020. CADINS in an Adult with Chronic Sinusitis and Atopic Disease. J. Clin. Immunol41: 256–258. [PubMed: 33057950]
41. Wang H, Yang H, Shivalila CS, Dawlaty MM, Cheng AW, Zhang F, and Jaenisch R. 2013. One-step generation of mice carrying mutations in multiple genes by CRISPR/Cas-mediated genome engineering. Cell153: 910–918. [PubMed: 23643243]
42. Moosbrugger-Martinz V, Schmuth M, and Dubrac S. 2017. A Mouse Model for Atopic Dermatitis Using Topical Application of Vitamin D3 or of Its Analog MC903. Methods Mol Biol1559: 91–106. [PubMed: 28063040]
43. Hamblet CE, Makowski SL, Tritapoe JM, and Pomerantz JL. 2016. NK Cell Maturation and Cytotoxicity Are Controlled by the Intramembrane Aspartyl Protease SPPL3. J. Immunol196: 2614–2626. [PubMed: 26851218]
44. Blonska M, and Lin X. 2009. CARMA1-mediated NF-kappaB and JNK activation in lymphocytes. Immunol. Rev228: 199–211. [PubMed: 19290929]
45. Baumgarth N2011. The double life of a B-1 cell: self-reactivity selects for protective effector functions. Nat. Rev. Immunol11: 34–46. [PubMed: 21151033]
46. Martin F, Oliver AM, and Kearney JF. 2001. Marginal zone and B1 B cells unite in the early response against T-independent blood-borne particulate antigens. Immunity14: 617–629. [PubMed: 11371363]
47. Cerutti A, Cols M, and Puga I. 2013. Marginal zone B cells: virtues of innate-like antibody-producing lymphocytes. Nature reviews. Immunology13: 118–132.
48. Appelgren D, Eriksson P, Ernerudh J, and Segelmark M. 2018. Marginal-Zone B-Cells Are Main Producers of IgM in Humans, and Are Reduced in Patients With Autoimmune Vasculitis. Frontiers in Immunology9.
49. Altin JA, Tian L, Liston A, Bertram EM, Goodnow CC, and Cook MC. 2011. Decreased T-cell receptor signaling through CARD11 differentially compromises forkhead box protein 3-positive regulatory versus T(H)2 effector cells to cause allergy. J. Allergy Clin. Immunol127: 1277–1285 e1275. [PubMed: 21320717]
50. Li M, Hener P, Zhang Z, Kato S, Metzger D, and Chambon P. 2006. Topical vitamin D3 and low-calcemic analogs induce thymic stromal lymphopoietin in mouse keratinocytes and trigger an atopic dermatitis. Proc Natl Acad Sci U S A103: 11736–11741. [PubMed: 16880407]
51. Adhikary PP, Tan Z, Page BDG, and Hedtrich S. 2021. TSLP as druggable target - a silver-lining for atopic diseases?Pharmacol. Ther217: 107648. [PubMed: 32758645]
52. Hara H, Ishihara C, Takeuchi A, Xue L, Morris SW, Penninger JM, Yoshida H, and Saito T. 2008. Cell type-specific regulation of ITAM-mediated NF-kappaB activation by the adaptors, CARMA1 and CARD9. J. Immunol181: 918–930. [PubMed: 18606643]

Author Manuscript Author Manuscript Author Manuscript Author Manuscript

53. Gross O, Grupp C, Steinberg C, Zimmermann S, Strasser D, Hannesschlager N, Reindl W, Jonsson H, Huo H, Littman DR, Peschel C, Yokoyama WM, Krug A, and Ruland J. 2008. Multiple ITAM-coupled NK-cell receptors engage the Bcl10/Malt1 complex via Carma1 for NF-kappaB and MAPK activation to selectively control cytokine production. Blood112: 2421–2428. [PubMed: 18192506]

54. Jamieson AM, Diefenbach A, McMahon CW, Xiong N, Carlyle JR, and Raulet DH. 2002. The role of the NKG2D immunoreceptor in immune cell activation and natural killing. Immunity17: 19–29. [PubMed: 12150888]

55. Beziat V, Jouanguy E, and Puel A. 2019. Dominant negative CARD11 mutations: Beyond atopy. J. Allergy Clin. Immunol143: 1345–1347. [PubMed: 30659853]

56. Newton K, and Dixit VM. 2003. Mice lacking the CARD of CARMA1 exhibit defective B lymphocyte development and impaired proliferation of their B and T lymphocytes. Curr. Biol13: 1247–1251. [PubMed: 12867037]

57. Garcia de Vinuesa C, O'Leary P, Sze DM, Toellner KM, and MacLennan IC. 1999. T-independent type 2 antigens induce B cell proliferation in multiple splenic sites, but exponential growth is confined to extrafollicular foci. Eur. J. Immunol29: 1314–1323. [PubMed: 10229099]

58. Sokol K, and Milner JD. 2018. The overlap between allergy and immunodeficiency. Curr Opin Pediatr30: 848–854. [PubMed: 30407976]

Author Manuscript Author Manuscript Author Manuscript Author Manuscript

Key Points

- CARD11$^{R30W/+}$ mice exhibit pathway-specific defects in T, B, and NK cells.
- CARD11$^{R30W/+}$ mice develop high IgE in an age-dependent manner with 50% penetrance.
- High IgE in CARD11$^{R30W/+}$ mice is uncoupled from Th2 expansion and atopic dermatitis.

Author Manuscript Author Manuscript Author Manuscript Author Manuscript

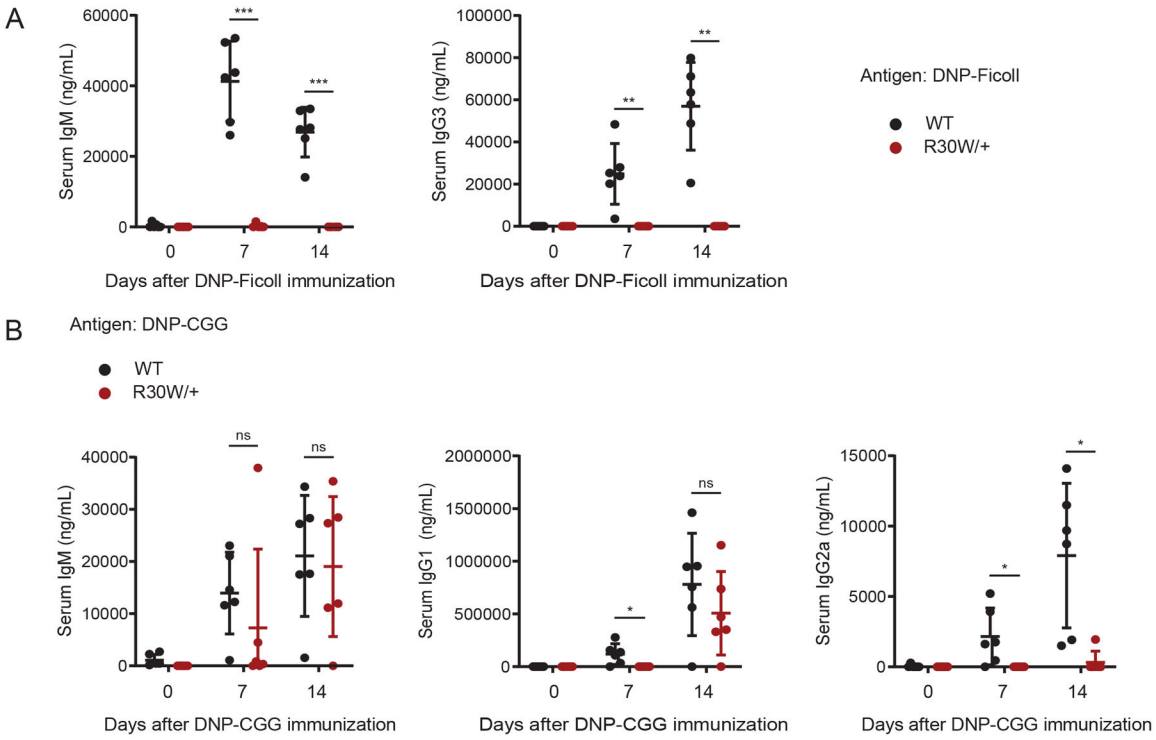

Figure 1.

The CARD11 R30W allele is sufficient to cause immunodeficiency. (A) DNP-specific IgM and IgG3 levels present in serum 7 and 14 days after immunization with DNP-Ficoll were measured by ELISA. (B) DNP-specific IgM, IgG1, and IgG2a levels present in serum 7 and 14 days after immunization with DNP-CGG were measured by ELISA. Each data point represents 1 mouse. Data are pooled from 3 independent experiments and N = 6 mice per genotype. ns not significant, * $p < 0.05$, ** $p < 0.01$, *** $p < 0.001$ (two-tailed unpaired t test with Welch's correction).

Author Manuscript Author Manuscript Author Manuscript Author Manuscript

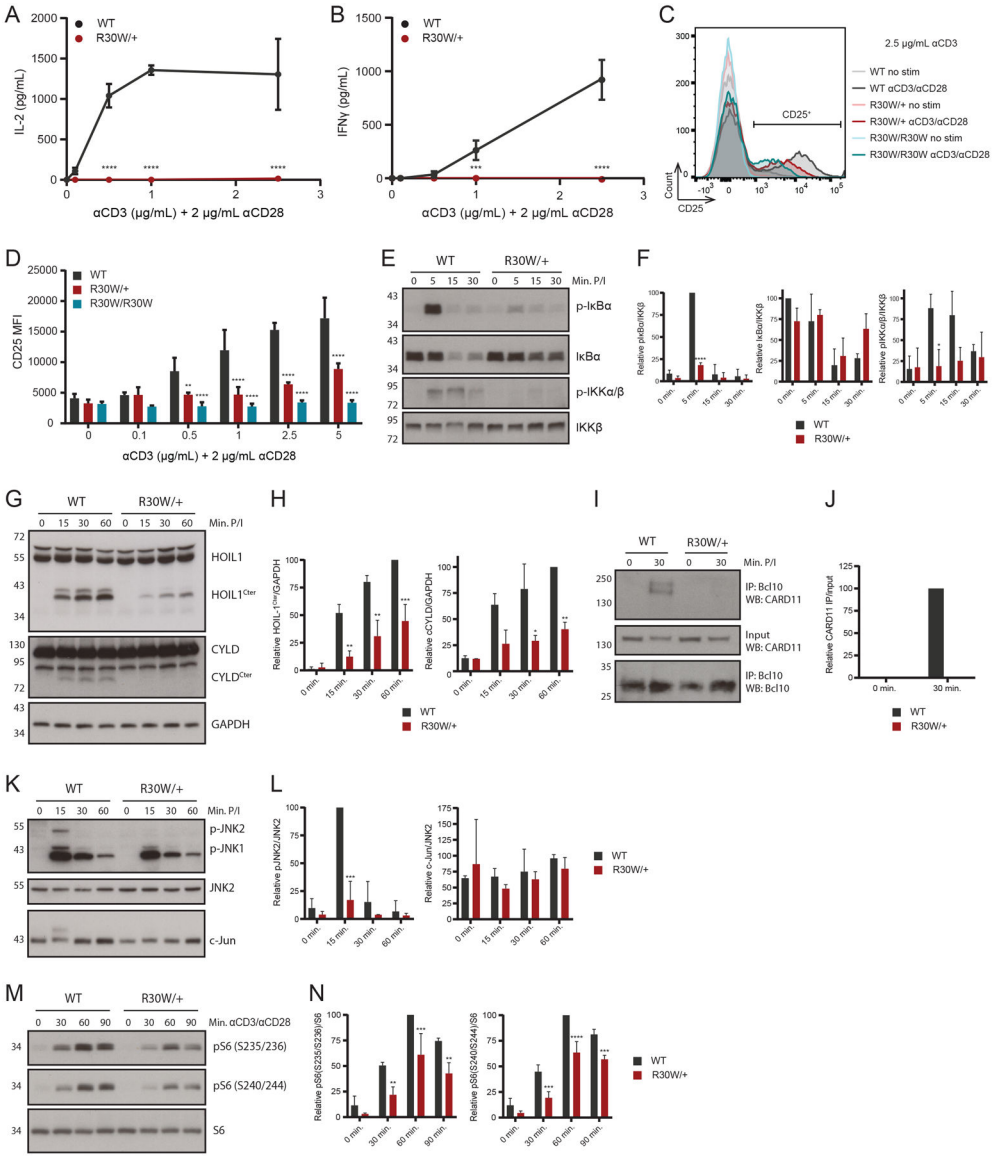

Figure 2.

Impaired activation and pathway-specific signaling defects in CARD11$^{R30W/+}$ T cells. (A) Splenic CD4^{+} T cells were stimulated with αCD3/αCD28 crosslinking at the indicated concentrations for 24 hours. IL-2 levels in culture media were measured by ELISA. (B) Splenic CD8^{+} T cells were stimulated with αCD3/αCD28 crosslinking at the indicated concentrations for 24 hours. IFNγ levels in culture media were measured by ELISA. (C) Splenic CD4^{+} T cells were stimulated with αCD3/αCD28 crosslinking at the concentrations indicated in (D) for 24 hours and CD25 surface expression was measured by flow cytometry. A representative flow cytometry plot showing CD25 expression after stimulation with 2.5 μg/mL αCD3 is shown here. (D) Mean fluorescence intensity (MFI) of the CD25^{+} gate is shown for each genotype at each concentration of αCD3 tested. (E, G, K) Splenic CD4^{+} T cells were stimulated with PMA/ionomycin for the indicated times. Lysates were analyzed by Western blotting with the indicated primary antibodies. (F) Quantification of

Author Manuscript Author Manuscript Author Manuscript Author Manuscript

NF-κB pathway signaling. The amount of phospho-IκBα, IκBα, and phospho-IKKα/β is normalized to the amount of IKKβ at each time point. (H) Quantification of induced MALT1 protease activity. The amount of HOIL-1^{Cter} and CYLD^{Cter} is normalized to the amount of GAPDH at each time point. (I) Splenic CD4^{+} T cells were stimulated with PMA/ionomycin for 30 minutes. Immunoprecipitation was performed with an anti-Bcl10 antibody as described in Materials and Methods and analyzed by Western blotting with the indicated primary antibodies. (J) Quantification of induced CARD11 binding to Bcl10. The amount of CARD11 in IP samples is normalized to the amount of CARD11 in input samples at each time point. (L) Quantification of JNK pathway signaling. The amount of phospho-JNK2 and c-Jun is normalized to the amount of JNK2 at each time point. (M) Splenic CD4^{+} T cells were stimulated with αCD3/αCD28 crosslinking for the indicated times. Lysates were analyzed by Western blotting with the indicated primary antibodies. (N) Quantification of mTORC1 pathway signaling. The amount of phospho-S6 (S235/S236) and phospho-S6 (S240/S244) is normalized to the amount of S6 ribosomal protein at each time point. All data are representative of 2–3 independent experiments. Western blot quantification is the average of 2–3 independent experiments. All experiments used 1 mouse per genotype except (I), which used 4 mice per genotype. * $p < 0.05$, ** $p < 0.01$, *** $p < 0.001$, *** $p < 0.0001$ (two-way ANOVA with Dunnett's multiple comparisons test).

Author Manuscript Author Manuscript Author Manuscript Author Manuscript

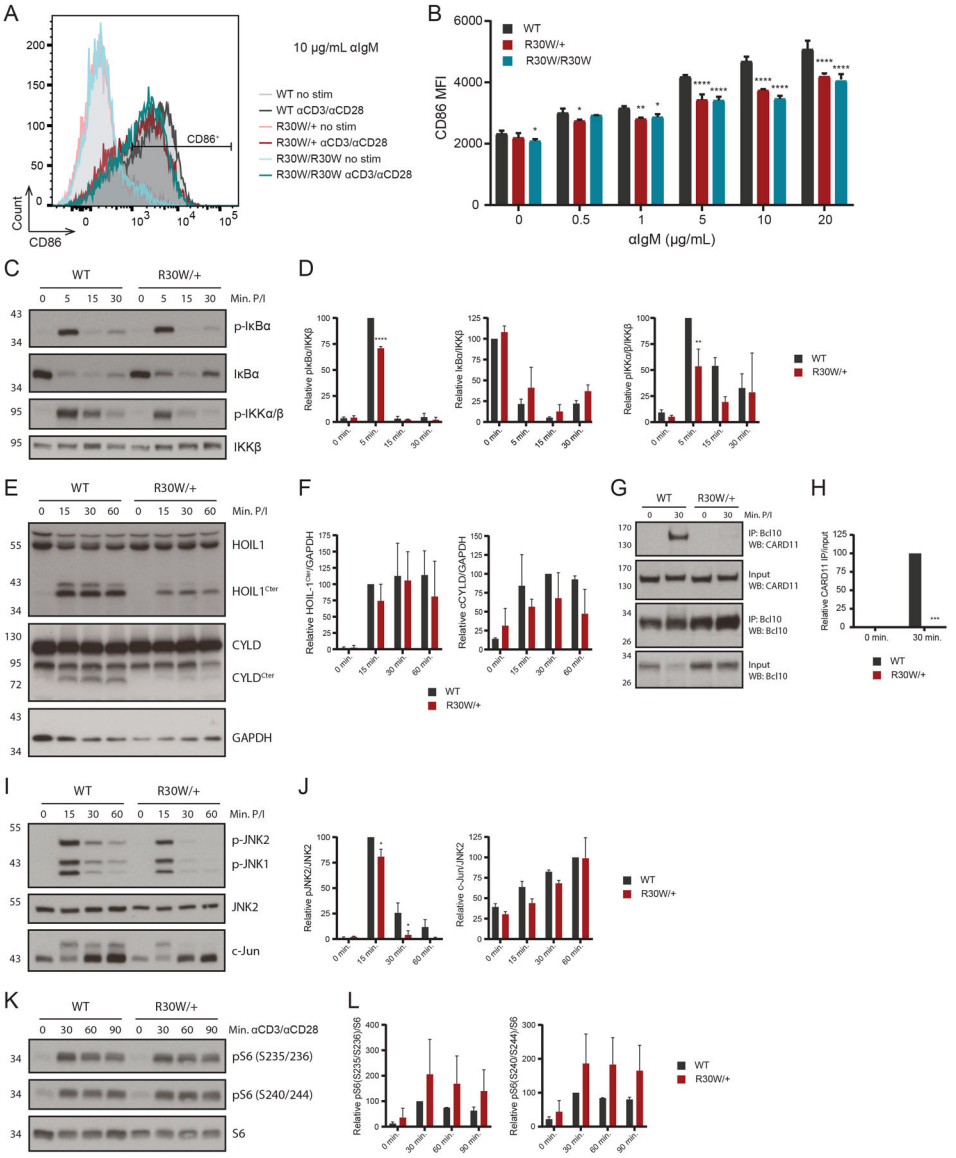

Figure 3.

Mild effects on activation and signaling in CARD11$^{R30W/+}$ B cells. (A) Splenic B cells were stimulated with αIgM at the concentrations indicated in (B) for 24 hours and CD86 surface expression was measured by flow cytometry. A representative flow cytometry plot showing the expression of CD86 after stimulation with 10 μg/mL αIgM is shown here. (B) MFI of the CD86^{+} gate is shown for each genotype at each concentration of αIgM tested. (C, E, I) Splenic B cells were stimulated with PMA/ionomycin for the indicated times. Lysates were analyzed by Western blotting with the indicated primary antibodies. (D) Quantification of NF-κB pathway signaling. The amount of phospho-IκBα, IκBα, and phospho-IKKα/β is normalized to the amount of IKKβ at each time point. (F) Quantification of induced MALT1 protease activity. The amount of HOIL-1^{Cter} and CYLD^{Cter} is normalized to the amount of GAPDH at each time point. (G) Splenic B cells were stimulated with PMA/ionomycin for 30 minutes. Immunoprecipitation was performed with an anti-Bcl10 antibody

Author Manuscript Author Manuscript Author Manuscript Author Manuscript

as described in Materials and Methods and analyzed by Western blotting with the indicated primary antibodies. (H) Quantification of induced CARD11 binding to Bcl10. The amount of CARD11 in IP samples is normalized to the amount of CARD11 in input samples at each time point. (J) Quantification of JNK pathway signaling. The amount of phospho-JNK2 and c-Jun is normalized to the amount of JNK2 at each time point. (K) Splenic B cells were stimulated with αIgM for the indicated times. Lysates were analyzed by Western blotting with the indicated primary antibodies. (L) Quantification of mTORC1 pathway signaling. The amount of phospho-S6 (S235/S236) and phospho-S6 (S240/S244) is normalized to the amount of S6 ribosomal protein at each time point. All data are representative of 2–3 independent experiments. Western blot quantification is the average of 2–3 independent experiments. All experiments used 1 mouse per genotype except (G), which used 3 mice per genotype. * $p < 0.05$, ** $p < 0.01$, *** $p < 0.001$, **** $p < 0.0001$ (two-way ANOVA with Dunnett's multiple comparisons test (all but (H)) or multiple t tests with Holm-Sidak correction (H)).

Author Manuscript
Author Manuscript
Author Manuscript
Author Manuscript

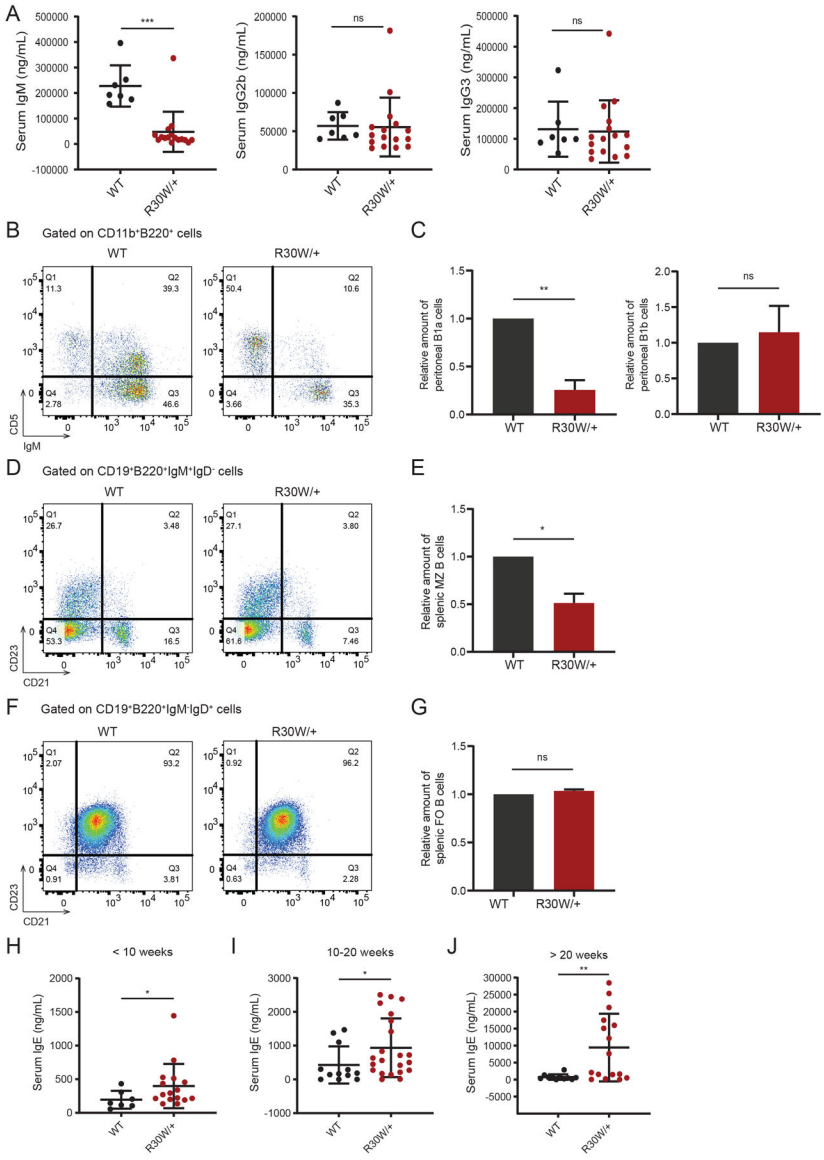

Figure 4.

Decreased serum IgM and age-dependent elevation of serum IgE with incomplete penetrance in CARD11$^{R30W/+}$ mice. (A) Basal serum IgM, IgG2b, and IgG3 levels were measured by ELISA in WT and CARD11$^{R30W/+}$ mice < 10 weeks old. (B) Representative flow cytometry plots showing the percentage of B1a and B1b cells in the peritoneal cavity of WT and CARD11$^{R30W/+}$ mice. Peritoneal cavity cells were gated on CD11b^{+}B220^{+} cells, and the quadrant gate shown was drawn using CD5 and IgM fluorescence minus one (FMO) controls. (C) Fraction of peritoneal CD11b^{+}B220^{+} cells that were CD5^{+}IgM^{+} B1a or CD5^{-}IgM^{+} B1b cells for each genotype normalized to the fraction observed in WT. (D and F) Representative flow cytometry plots showing the percentage of splenic marginal zone (D) or follicular (F) B cells in WT and CARD11$^{R30W/+}$ mice. Splenocytes were gated on CD19^{+}B220^{+}IgM^{+}IgD^{-} (D) or CD19^{+}B220^{+}IgM^{-}IgD^{+} (F) cells, and the quadrant gates shown were drawn using CD23 and CD21 FMO controls. (E) Fraction

Author Manuscript Author Manuscript Author Manuscript Author Manuscript

of splenic $CD19^{+}B220^{+}IgM^{+}IgD^{-}$ cells that were $CD23^{-}CD21^{hi}$ marginal zone B cells for each genotype normalized to the fraction observed in WT. (G) Fraction of splenic $CD19^{+}B220^{+}IgM^{-}IgD^{+}$ cells that were $CD23^{+}CD21^{int}$ follicular B cells for each genotype normalized to the fraction observed in WT. (H-J) Basal serum IgE levels were measured by ELISA in WT and $CARD11^{R30W/+}$ mice < 10 weeks old (H), between 10 and 20 weeks old (I), and > 20 weeks old (J). In (A) and (H-J), each data point represents 1 mouse, and N = 7–22 mice per genotype. In (C), (E), and (G), data are the average of at least 3 independent experiments and 1 mouse per genotype was used for each experiment. ns not significant, * $p < 0.05$, ** $p < 0.01$, *** $p < 0.001$ (two-tailed unpaired t test with Welch's correction).

Author Manuscript Author Manuscript Author Manuscript Author Manuscript

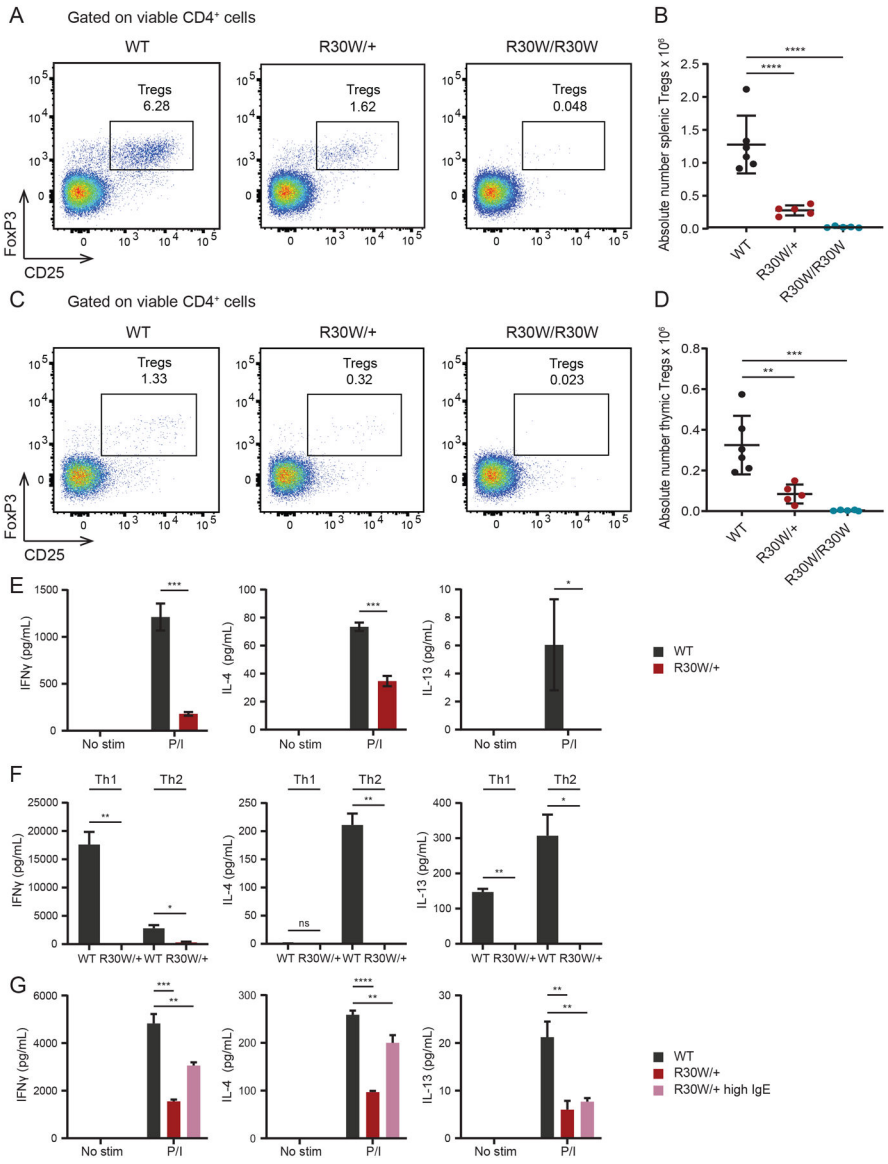

Figure 5.

The CARD11 R30W allele causes a significant loss of regulatory T cells without a concomitant Th2 expansion. (A) Representative flow cytometry plots showing the percentage of splenic Tregs in WT, CARD11$^{R30W/+}$, or CARD11$^{R30W/R30W}$ mice. Splenocytes were gated on viable CD4$^+$ T cells, and the Treg gate was drawn using CD25 and FoxP3 FMO controls. (B) Absolute numbers of splenic CD3$^+$CD4$^+$CD25$^+$FoxP3$^+$ Tregs for each genotype. (C) Representative flow cytometry plots showing the percentage of thymic Tregs in WT, CARD11$^{R30W/+}$, or CARD11$^{R30W/R30W}$ mice. Thymocytes were gated on viable CD4$^+$ T cells, and the Treg gate was drawn using CD25 and FoxP3 FMO controls. (D) Absolute numbers of thymic CD4$^+$CD8$^-$CD25$^+$FoxP3$^+$ Tregs for each genotype. (E) Splenic CD4$^+$ T cells from WT and CARD11$^{R30W/+}$ mice < 10 weeks old were stimulated with PMA/ionomycin for 24 hours. Levels of IFN**γ**, IL-4, and IL-13 in culture media were measured by ELISA. (F) Naïve splenic CD4$^+$ T cells from WT and CARD11$^{R30W/+}$ mice

Author Manuscript Author Manuscript Author Manuscript Author Manuscript

< 10 weeks old were differentiated to Th1 or Th2 subtypes in culture as described in Materials and Methods. Differentiated cells were restimulated with αCD3 for 24 hours, and the amount of IFNγ, IL-4, or IL-13 in culture media was measured by ELISA. (G) Splenic $CD4^+$ T cells from WT, $CARD11^{R30W/+}$ mice with normal IgE, and $CARD11^{R30W/+}$ mice with high IgE > 20 weeks old were stimulated with PMA/ionomycin for 24 hours. Levels of IFNγ, IL-4, and IL-13 in culture media were measured by ELISA. In (B) and (D), each data point represents 1 mouse. Data is pooled from at least 3 independent experiments and N = 5–6 mice per genotype. In (E-G), all data are representative of at least 2 independent experiments, and 1–2 mice per genotype were used for each experiment. * $p < 0.05$, ** $p < 0.01$, *** $p < 0.001$, **** $p < 0.0001$ (one-way ANOVA with Dunnett's multiple comparisons test (B and D) or two-tailed unpaired t test with Welch's correction (E-G)).

Author Manuscript Author Manuscript Author Manuscript Author Manuscript

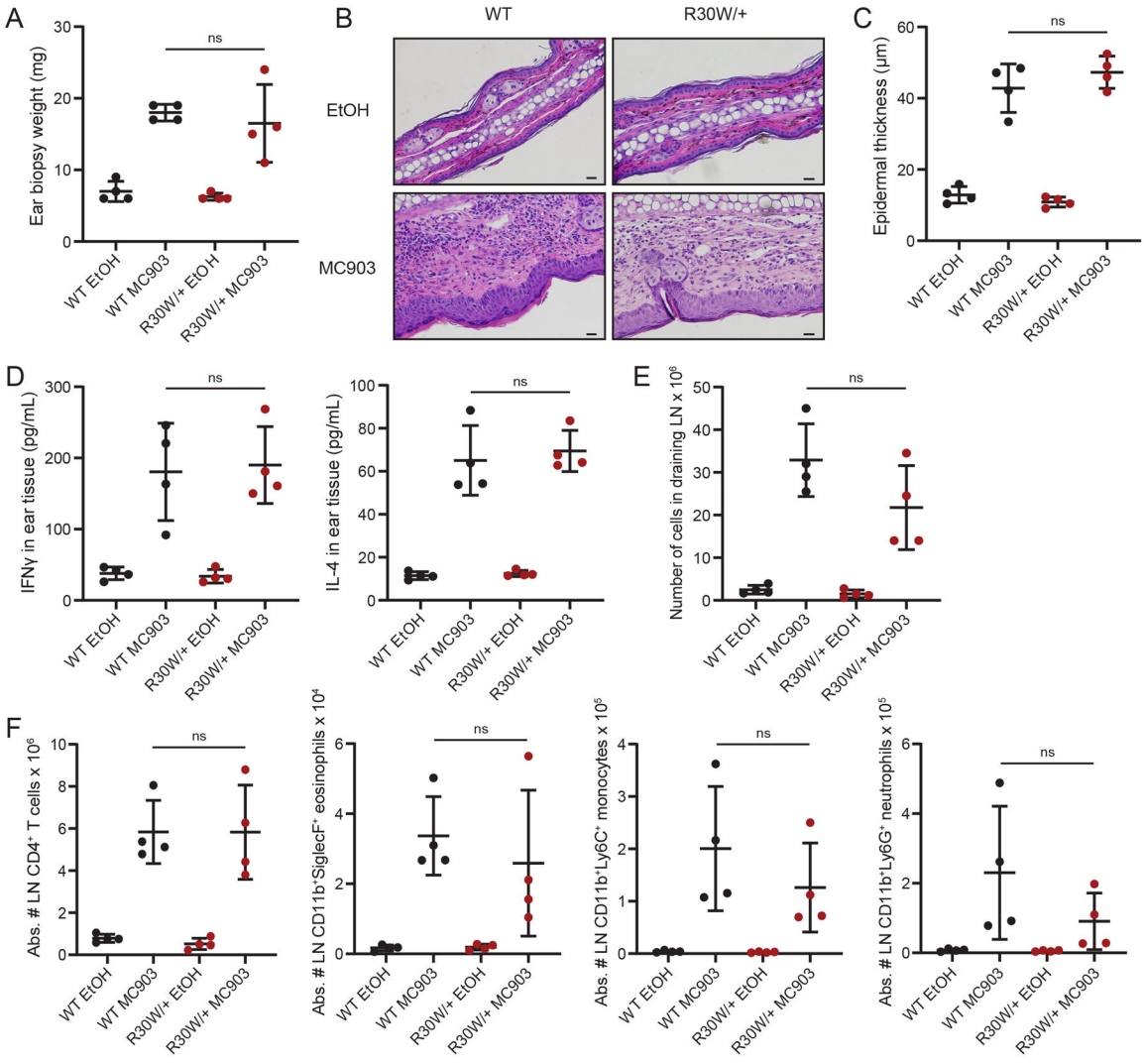

Figure 6.

WT and CARD11$^{R30W/+}$ mice respond similarly to treatment with the vitamin D analog MC903. (A) Weight, in mg, of 6 mm punch biopsies taken from mouse ears treated with either ethanol (EtOH) or MC903. (B) Representative histology (H&E stain) of mouse ear tissue after EtOH or MC903 treatment. Scale bar = 20 μm. (C) Epidermal thickness of ear tissue after treatment with EtOH or MC903 was measured from histology images using ImageJ software. (D) Protein was extracted from ear tissue as described in Materials and Methods and levels of IFNγ and IL-4 in the extract were measured by ELISA. (E) Total number of cells in the draining lymph node (LN) of mice treated with EtOH or MC903. (F) Absolute numbers of CD4$^+$ T cells, CD11b$^+$SiglecF$^+$ eosinophils, CD11b$^+$Ly6C$^+$ monocytes, and CD11b$^+$Ly6G$^+$ neutrophils present in the draining LN after treatment with EtOH or MC903 were determined by flow cytometry. In (A) and (C-F), each data point represents 1 mouse. Data are pooled from 2 independent experiments and N = 4 mice per treatment condition. ns not significant (two-tailed unpaired t test with Welch's correction).

Author Manuscript
Author Manuscript
Author Manuscript
Author Manuscript

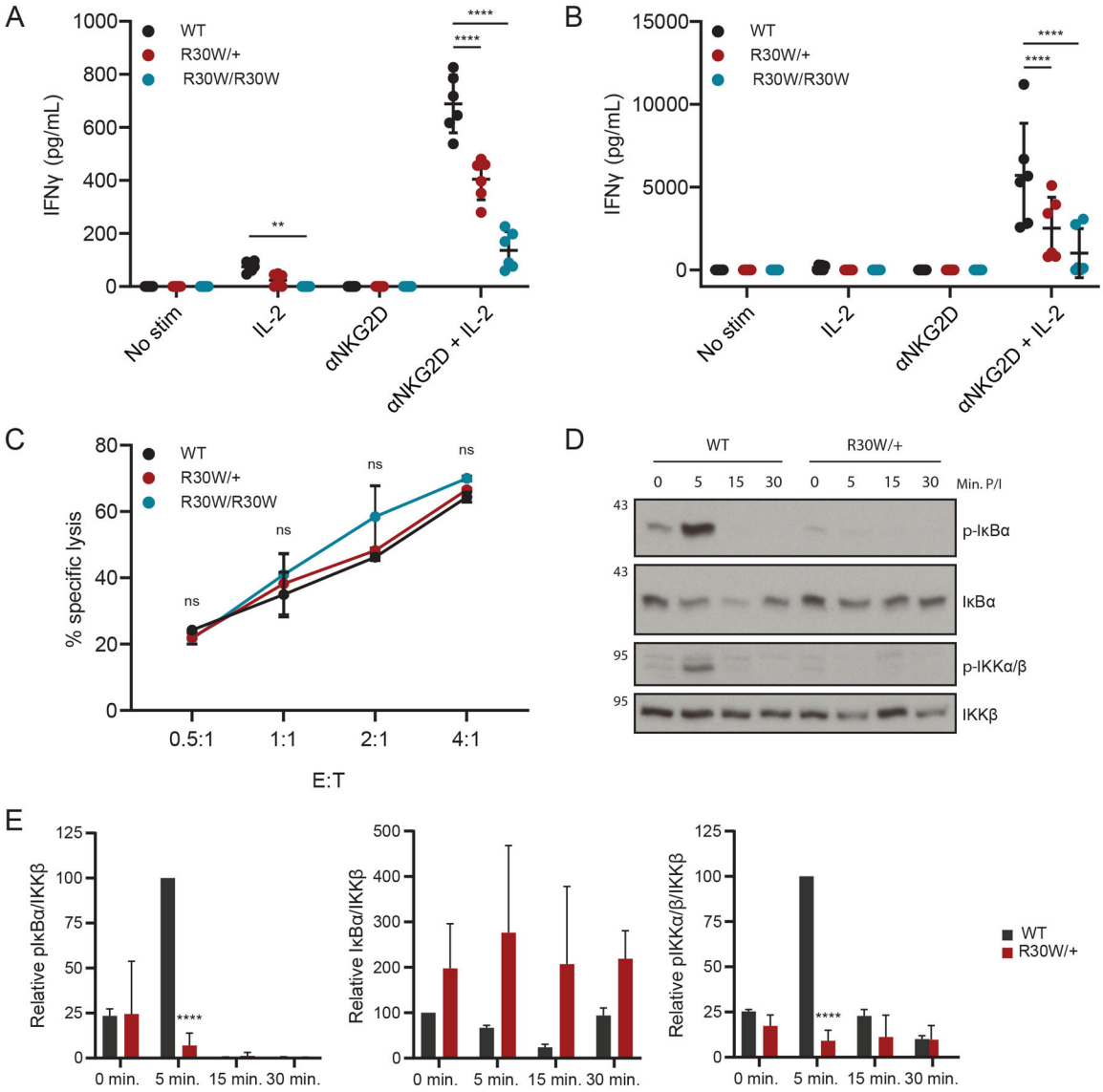

Figure 7.

The CARD11 R30W allele causes pathway-specific defects in NK cell function. (A) Freshly isolated splenic NK cells were stimulated with αNKG2D in the presence of IL-2 for 24 hours. Levels of IFNγ in culture media were measured by ELISA. (B) Splenic NK cells were expanded in culture for 6 days in the presence of IL-15, then stimulated with αNKG2D in the presence of IL-2 for 24 hours. Levels of IFNγ in culture media were measured by ELISA. (C) Equivalent numbers of $NK1.1^{+}CD49b^{+}$ splenic NK cells were co-cultured with CFSE-loaded YAC-1 cells for 4 hours in the indicated E:T ratios. The percentage of $CFSE^{+}$Annexin V^{+} cells at each E:T ratio was determined by flow cytometry and is reported as the percent specific lysis. (D) Splenic NK cells were expanded in culture for 6 days in the presence of IL-15, then stimulated with PMA/ionomycin for the indicated times. Lysates were analyzed by Western blotting with the indicated primary antibodies. (E) Quantification of NF-κB pathway signaling. The amount of phospho-IκBα, IκBα, and phospho-IKKα/β is normalized to the amount of IKKβ at each time point. In (A) and (B), data are pooled

Author Manuscript Author Manuscript Author Manuscript Author Manuscript

from 2 independent experiments, and each data point represents a well of cultured NK cells. In (C) and (D), data are representative of at least 2 independent experiments. Western blot quantification is the average of 2 independent experiments. All experiments used 1–2 mice per genotype. ns not significant, ** $p < 0.01$, **** $p < 0.0001$ (two-way ANOVA with Dunnett's multiple comparisons test).